Sources and formation of nucleation mode particles in remote tropical marine atmospheres over the South China Sea and the Northwest Paci fic Ocean

Shen, Yanjie

2020-09-15

Shen , Y , Wang , J , Gao , Y , Chan , C K , Zhu , Y , Gao , H , Petaja , T & Yao , X 2020 , ' Sources and formation of nucleation mode particles in remote tropical marine atmospheres over the South China Sea and the Northwest Paci fic Ocean ' , The Science of the Total Environment , vol. 735 , 139302 . https://doi.org/10.1016/j.scitotenv.2020.139302

http://hdl.handle.net/10138/343551
https://doi.org/10.1016/j.scitotenv.2020.139302

Sources and formation of nucleation mode particles in remote tropical marine atmospheres over the South China Sea and the Northwest Pacific Ocean

Yanjie Shen[a], Juntao Wang[a], Yang Gao[a, b], Chak K. Chan[c]*, Yujiao Zhu[a], Huiwang Gao[a, b], Tuukka Petäjä[d,e], Xiaohong Yao[a, b]*

[a] Key Lab of Marine Environmental Science and Ecology (MoE)/ Institute for Advanced Ocean Study, Ocean University of China, Qingdao, 266100, China.

[b] Laboratory for Marine Ecology and Environmental Sciences, Qingdao National Laboratory for Marine Science and Technology, Qingdao, 266237, China.

[c] School of Energy and Environment, City University of Hong Kong, Hong Kong, 999077, China.

[d] Joint International Research Laboratory of Atmospheric and Earth System Sciences, School of Atmospheric Sciences, Nanjing University, Nanjing, China.

[e] Institute for Atmospheric and Earth System Research/Physics, Faculty of Science, University of Helsinki, FI-00014, Finland.

*Corresponding author: X. H. Yao (xhyao@ouc.edu.cn) and C. K. Chan (chak.k.chan@cityu.edu.hk)

Highlights:

- Strong and weak local turbulence-driven NPF events were observed over SCS.
- A clear nucleation particle mode was observed over the tropical zone of NWPO.
- No growth of the nucleation mode was detected. This could indicate limited abundance of key precursors.

Abstract

A fast mobility particle sizer operating at a one-second time resolution was used to measure aerosol particle number size distribution (5.6-560 nm) in marine conditions over the South China Sea (SCS) from 29 March to 2 May 2017 and in the tropic zone of the Northwest Pacific Ocean (NWPO) from 10 to 29 October 2018. The clean background number concentration of nucleation mode atmospheric particles (<30 nm) was approximately 0.6×10^{3} cm^{-3} in these areas. Two nighttime and five daytime strong new particle formation (NPF) events were observed to occur extending over a spatial scale from 2-140 km in the SCS, with a net increase of nucleation mode particles of 4.5×10^{4} cm^{-3}$\pm$$3.4\times10^{4}$ cm^{-3} during five of the seven events. Nighttime NPF events were unlikely associated with sulfuric acid vapor because of lack of photochemical reactions. Daytime NPF events share several common features with nighttime NPF events, e.g., dramatic spatiotemporal variations in the number concentration of the nucleation mode particles. Without aerosol precursor measurements we cannot address the vapors driving the formation process. However, our results show no banana-shaped growth of the particles. The growth into larger particle sizes seem to be restricted by the availability of condensable components in the gas phase. The nucleation mode was observed and sometimes even dominated the number concentration over other particle modes in the marine atmosphere over the tropic zone of the NWPO. In addition, more data obtained during the two campaigns and other campaigns were also applied to strengthen the analysis in terms of origins, formation and absent growth of nucleation mode particles in the marine atmospheres over the two tropic zones.

Key words: new particle formation; tropical marine atmosphere; dramatic; SCS; NWPO

1. Introduction

New particle formation (NPF) is a common atmospheric phenomenon that has been observed globally in various continental and marine environments (Kulmala et al. 2004; Gong et al., 2010; Liu et al., 2008; O'Dowd et al., 2002a,b; Liu et al., 2014; Xiao et al., 2015; Xie et al., 2015; Yu et al., 2015; Zhu et al., 2017; Kerminen et al., 2018; Chu et al., 2019). NPF includes atmospheric nucleation and particle growth, and the grown new particles are proposed to affect the climate by directly scattering sunlight or indirectly affecting cloud formation (Kulmala et al., 2004; Kerminen et al., 2012; Zhang et al., 2012). In the boundary layer of continental atmospheres, sulfuric acid vapor is widely recognized as the necessary precursor for atmospheric nucleation, and NH_3, amines and organics have been reported to greatly enhance atmospheric nucleation (Kulmala et al., 2004; Zhang et al., 2004; Nieminen et al., 2018; Yao et al., 2019). In the boundary layer of marine and coastal atmospheres, the oxidation products of dimethyl sulfide (DMS) such as sulfuric acid as well as reactive iodine compounds are proposed to induce atmospheric nucleation (O'Dowd et al., 2002a,b; Quinn & Bates, 2011, Sipilä et al. 2016). In the free troposphere, ion-induced nucleation can also play a role (English et al., 2011). Relative to the abundant observations in the continental atmospheric boundary layer, observations of the occurrence of NPF in the marine atmospheric boundary layer are scarce (Sellegri et al., 2016; Nieminen et al., 2018). However, oceans cover almost 70% of the earth's surface and tropical oceans are the major moisture source in the global atmosphere because of the strong evaporation associated with high surface sea water temperature (Deng et al., 2014; John et al., 2009). Studies of NPF in tropical marine atmospheres and their potential impact on the climate are even more limited (Ueda et al., 2016; Williamson et al., 2019).

Sulfuric acid vapor has been reported to induce NPF events in clean and polluted marine atmospheres (Leaitch et al., 2013; Croft et al., 2016). The vapor can be generated from the oxidation of marine biogenic precursors or from the long-range transport of continental air pollutants, depending on the sources of air masses. NPF events associated with sulfuric acid vapor in the marine atmosphere usually display a classical banana-shaped growth of new particles in the particle number-size distribution data contour plot (Chang et al., 2011; Liu et al., 2014; Guo et al., 2016; Ueda et al., 2016). Moreover, airborne flight observations indicated NPF events could occur at different altitudes, ranging from the well-mixed planetary boundary layer to the lower free troposphere in urban and coastal areas. It is also possible that the observed NPF events occur aloft and then transport down to the marine boundary layer, near sea level (Weber et al., 1999; Meng et al., 2015; Sanchez et al., 2018; Williamson et al., 2019). In such cases, it is difficult to determine the apparent formation rate of new particles and strength of NPF events based on the observed particle number concentrations near sea level.

Reactive iodine compounds have been frequently reported to induce NPF in coastal areas (Allan et al., 2015; Ehn et al., 2010a; Huang et al., 2010a; McFiggans et al., 2010; O'Dowd et al., 2010; O 'dowd et al., 2002a; Sipilä et al., 2016). Marine emissions of reactive iodine compounds occur in coastal areas and in open ocean environments (O'Dowd et al., 2002b; Sipilä et al., 2016). Due to the limited studies, direct evidence is insufficient to support iodine compounds acting as major precursors for NPF in remote marine atmospheres (Allan et al., 2015; Sellegri et al., 2016). In the literature, a small fraction of these NPF events driven by iodine compounds display the classical banana-shaped particle growth (O'Dowd et al., 2010; O'Dowd et al., 2002a; Ehn et al., 2010). During most of the NPF events driven by iodine compounds, the geometric median diameter (GMD) of newly formed particles was smaller than 10-20 nm and no apparent growth of new particles was found. What determines the absence of apparent growth of particles < 10-20 nm is unclear. Zhu et al (2014) and Man et al. (2015) reported a ceiling of 30-50 nm for the growth of newly formed particles in Qingdao and Hong Kong and correlated these observations to insufficient condensation of ammonium nitrate.

In this study, a fast mobility particle sizer (FMPS) and a condensation particle counter (CPC) were used to measure the particle number size distributions during a cruise campaign over the South China Sea (SCS) and a cruise campaign over the tropic zone of the Northwest Pacific Ocean (NWPO). The NWPO has been projected to experience the greatest increases in sea surface temperature and CO_2 input under a future warming climate (John et al., 2015; Lauvset et al., 2017). NPF and aerosol-cloud interactions associated may be even more important therein than in other tropic marine atmospheres. The tropic zone of NWPO and the SCS are separated by Philippines, but their water bodies have a large difference on oligotrophic levels. A comparison study of NPF events therein is highly valuable. Taking advantage of the high time resolution data obtained (Yao et al., 2005; Liu et al., 2014), we first isolated NPF events induced by self-vessel emissions in the tropical marine atmosphere to identify NPF events observed only in the atmosphere over the SCS. Different from well-documented features in NPF events in the continental atmosphere, these NPF events over the SCS exhibit some common features such as the occurrence at ambient RH higher than 70%, dramatic spatiotemporal variations in the number concentration of nucleation mode particles, and the absence of banana-shaped growth of new particles. We introduced the coefficient of variation (CV) of the particle number concentration to analyze the causes of the dramatic variations in the number concentration of new particles. We also introduced the maximum increase in the concentration of newly formed particles to characterize these NPF events since the conventionally adopted formation rate of new particles cannot work properly because of dramatic fluctuation of new particles in number concentration. In addition, we conducted a comparative analysis of identified NPF events with those previously reported in the rural coastal atmosphere adjacent to the SCS and previously observed in the sub-tropic zone of the remote NWPO. The results were discussed in terms of factors induced NPF and chemicals determined particle growth, etc. The observations are all compared with those in the marine atmosphere over the tropic zone of the NWPO. This study provides new insights on occurrence and drivers of NPF and origins of nucleation mode particles in tropical marine atmospheres.

2. Materials and Methods

2.1. Cruise route and instruments

From 29 March to 2 May 2017, a cruise campaign across the SCS was organized by the National Natural Science Foundation of China using the research vessel *Shiyan-1*. The route is shown in Fig. 1a. A Fast Mobility Particle Sizer (FMPS, TSI, 3091) downstream of a dryer (TSI, 3062) was set on the top floor, approximately 10 m above sea level, to measure the concentrations of marine atmospheric particles from 5.6 nm to 560 nm in 32 channels at a one-second time resolution. A condensation particle counter (CPC, TSI, 3785） shared a splitter with the FMPS and simultaneously operated at a two-second time resolution. The CPC data are used to correct the data measured by the FMPS (Zimmerman et al., 2015). A Droplet Measurement Technologies continuous flow cloud condensation nuclei counter (CCNC, DMT, 100) was used to measure the bulk cloud condensation nuclei (CCN) concentration at five different supersaturation (SS) conditions of 0.05%, 0.1%, 0.2%, 0.4% and 0.6%. In addition, a fourteen-stage Nano MOUDI-II was used to collect atmospheric particles from 0.01 to18 μm to analyze the aerosol chemical composition. Nine MOUDI samples were collected at a flow rate of 29.4 $L \cdot min^{-1}$. The sampling duration was generally longer than 10 hours but varied depending on the rough estimation from on-board measured size-segregated particle number concentrations. A detailed chemical analysis has been described by Hu et al. (2015) and Xie et al. (2018). In addition, meteorological data, including wind speed (WS), wind direction (WD), ambient temperature (T) and relative humidity (RH) were measured continuously on board.

Datasets obtained during two spring cruise campaigns across the sub-tropic oceanic zone of the NWPO in 2014 (18 March to 21 April) and 2016 (25 March to 22 April) were used for comparative analysis and the cruise routes are shown in Fig. 1b. A FMPS and a Nano Scanning Mobility Particle Sizer Spectrometer (SMPS) nanoparticle sizer (TSI, 3910) were used to measure the concentrations of marine atmospheric particles on the 2014 and 2016 cruise campaigns, respectively. In addition, NPF events on the eastern coastline of Hong Kong in 2011 that were previously reported by Man et al. (2015) were included for comparison with those observed across the SCS.

FMPS and CPC datasets obtained onboard the research vessel *Kexue* during a cruise campaign across the tropic oceanic zone of the NWPO on 10-29 October 2018 were also analyzed (Fig. S1). The number concentrations of particles <10 nm during the campaign were excluded for analysis because of their noisy signals. Such noisy signals were not observed for the number concentrations of particles ≥10 nm and the concentrations were normal in comparison with those measured during other cruise campaigns. The FMPS was out of service after 29 October because of severe weather conditions.

2.2. Computational methods

In this study, the size distribution of newly formed particles was fitted by multiple log-normal distribution functions (Whitby, 1978; Zhu et al., 2014). The apparent growth rate (GR) of newly formed particles was calculated as:

$$GR = \frac{\Delta D_P}{\Delta t}$$

where ΔD_p is the increased median mobility diameter of the new particle mode and Δt is the duration of the growth of newly formed particles. The GR of preexisting particles before NPF events was also calculated using this method.

Moreover, measurements averaged over each 30 s period were used to calculate the coefficient of variation (CV, equal to the standard deviation over the mean concentration in each 30 s interval), which has been demonstrated to be useful for describing the transport of aerosol particles (Meng et al., 2015). In this study, we calculated the CV of the 5.6-30 nm and 30-100 nm particle number concentrations ($N_{<30}$ and N_{30-100}, respectively) and a t-test was used to assess the statistical significance (p<0.05). The CV ratio, defined as CV of $N_{<30}$ ($CV_{N<30}$) over CV of N_{30-100} ($CV_{N30-100}$) was also computed. We combined the CV values for different sized particles and the CV ratios during, before, and after the NPF events to analyze the causes of dramatic spatiotemporal variations in number concentration of new particles.

The net maximum increase in the nucleation mode particle number concentration (NMINP) was calculated as $N_{<30}\ (t1) - N_{<30}\ (t0)$. $N_{<30}\ (t0)$ is the nucleation mode particle number concentration immediately before the apparent NPF initialization. Depending on the characteristics of the NPF events, $N_{<30}\ (t1)$ can be calculated in two ways (Zhu et al., 2017). For NPF events with a relatively smooth and single temporal peak nucleation mode particle number concentration, the maximum concentration is used; this method is referred to as Method 1. For NPF events with multiple peaks in the temporal profile of the nucleation mode particle number concentration, it is defined as the average of the top 10 percentile values of these peaks (referred to as Method 2). In the SCS, the NPF events fall into the second case and hence Method 2 was used. However, the NPF events in the NWPO and Hong Kong (Man et al. 2015) fall into the first case and Method 1 was used. Formation rate of newly formed particles (FR) is calculated by NMINP over t_1-t_0.

In addition, the 24-hour air mass back trajectories were calculated by using the Hybrid Single-Particle Lagrangian Integrated Trajectory (HYSPLIT) model from the NOAA Air Resources Laboratory to investigate the origins of air masses. The 6-hourly 24-hour backward trajectories at 100 m, 500 m and 1000 m above mean sea level (a.m.s.l.) were calculated at the initial NPF time on NPF days (Fig. S2).

3. Results and discussion

3.1. Separating NPF events from combustion plumes in marine atmospheres

Ship combustion plumes released by the research vessel itself or other marine traffic contain a large amount of primary particles and can greatly increase the particle concentrations in the marine atmosphere (Li et al., 2015; Liu et al., 2014; Ueda et al., 2016). In addition to the primary particles, ship combustion may release large amounts of gases such as SO_2, particularly from ships using heavy oil or high sulfur-content diesel (i.e., 0.5-1.0% sulfur-content diesel in China). Under favorable meteorological conditions, secondary formation of atmospheric particles in freshly diluted ship plumes is also expected. Thus, it is essential to identify the primary and secondary particle signals associated with self-vessel plumes and nucleation mode particles unrelated to self-vessel plumes. Primary and secondary particles derived from other marine traffic plumes have become part of ambient aerosols in marine atmospheres and are therefore included in our analysis. They are included as part of non self-vessel events in the discussions below. The separation method is explained in more detail below.

As shown in Figs. 2a and 2b, a plume (marked with red rectangle in Fig. 2a) with geometric median mobility diameter (GMD) of particles of 50±10 nm was observed from 10:25 to 16:45 (Beijing local standard time) on 15 April 2017. The research vessel traveled approximately 20 km during the period (Fig. 2e), implying that the plume is most likely regional. A few spikes of N_{30-100} superimposed on the plume occurred from 11:45 to 12:10 (Fig. 2b, marked with green rectangle) and the GMD of particles in the spikes was as high as 60±10 nm (Fig. 2a). A number of spikes were also observed from 15:20 to 16:40 and from 19:20 to 21:15 (Fig. 2b, marked with purple rectangle), for which the GMD of particles was also 60±10 nm. The spikes lasted only from several minutes to ten minutes. Considering the almost invariant large GMD of the particles and the largely increased N_{30-100} (0.9×10^4-5.2×10^4 cm^{-3}) in spikes against the clear background (770±199 cm^{-3} on that day), the spikes were very likely caused by primary self-vessel emissions, superimposed onto the regional plume. Note that there was no increase in $N_{<30}$ in these N_{30-100} spikes on that day. A few spikes in $N_{<30}$ were observed from 12:45 to 14:05 (with the vessel traveling for ~3 km, red line in Fig. 2e) but there was no significant correlation between N_{30-100} and $N_{<30}$ at 95% confidence (top right of Fig. 2b). Moreover, the net increase in $N_{<30}$ of each spike was much larger than that in N_{30-100} simultaneously measured during the period. However, the reverse is true in self-vessel-induced NPF events because of large condensation sink as shown in Figs. 2c and 2d and discussed in the next paragraph. Thus, these spikes in $N_{<30}$ were more likely ascribed to non self-vessel-induced NPF events, in which the nucleation mode particles had the GMD at 11±0.3 nm and NMINP of 2.1×10^4 cm^{-3}. Nighttime NPF event was not observed on that day.

Self-vessel induced NPF events indeed occur for sometimes through the whole campaign (Fig. S3). We further characterized self-vessel induced NPF in order to distinguish from non self-vessel-induced NPF events abovementioned. Dozens of spikes in $N_{<30}$ observed on 5 April 2017, as shown in Figs. 2c and 2d, were used to illustrate and nucleation mode particles in spikes had their GMD at 9.0±0.3 nm instead of 11±0.3 nm observed in non self-vessel-induced NPF events. Even more spikes in $N_{30\text{-}100}$ were observed on 5 April 2017, but some were observed also in the absence of spikes in $N_{<30}$. Again, the almost invariant GMD of particles at approximately 60 nm in these spikes implied that primary self-vessel emissions probably overwhelmingly contributed to the $N_{30\text{-}100}$ spikes. Notably, some spikes in $N_{30\text{-}100}$ occurred simultaneously with spikes in $N_{<30}$, with a significant correlation at 95% confidence (right top of Fig. 2d), unlike those spikes from non self-vessel emissions as shown in top right of Fig. 2b. These spikes in $N_{<30}$ should be ascribed to the nucleation of primarily-emitted sulfuric acid in diluted self-vessel plumes. Fresh ship plumes always contain sulfuric acid and organic vapors produced from combustion. The formation of nucleation mode particles in ship plumes relies on the balance of the availability of sulfuric acid and organic vapors for nucleation against the condensation sink. However, $N_{<30}$ was only 1/3-1/2 of $N_{30\text{-}100}$ in presence of spikes of $N_{<30}$ in self-vessel plumes because of the large condensation sink associated with those accumulation mode particles (Fig. 2d). Thus, largely increased $N_{30\text{-}100}$ was also used as an indicator for anthropogenic combustion emissions in the marine atmosphere. We conducted a similar analysis for the data collected throughout the entire campaign. Seven strong non self-vessel-induced NPF events were identified with $N_{<30}$ generally above 1×10^4 cm^{-3}. (Figs. 1a, 3 and S3) and are discussed in detail in section 3.2-3.4. A number of weak non self-vessel-induced NPF events were also observed at different times, with $N_{<30}$ decreased by approximately one order of magnitude. Only the one occurring immediately after a strong NPF event on 15 April and the longest non-continuous weak NPF event on April 27-28 were selected for analysis in Section 3.5. In the particular events, $N_{<30}$ were comparable to those during NPF events observed in the clean marine atmosphere over the North Pacific Ocean reported by Ueda et al (2016).

During the cruise campaign over the tropic oceanic zone of the NWPO in 2018, the GMD of particles derived from self-vessel plumes were generally 32±4 nm, with an exception of 28±3 nm only during five hours at 12:13-17:03 on 25 October 2018 (Fig. S1). The exception was not yet to be explained. Self-vessel plumes were less frequently detected because the FMPS was not situated downwind of the vessel smoke stack under most of wind conditions.

In summary, self-vessel NPF events are characterized by coexisting spikes of $N_{<30}$ and N_{30-100} and the net increase in $N_{<30}$ was approximately only 1/3-1/2 that in N_{30-100}; non self-vessel NPF events are characterized by either absence of spikes of N_{30-100} or the net increase in $N_{<30}$ to be much larger than that in N_{30-100}.

3.2. Overview of strong NPF events observed across the SCS

If not specified, NPF events presented in Section 3.2-3.4 are categorized as strong events, with characteristics of either absence of spikes of N_{30-100} or the large net increase in $N_{<30}$. Seven non self-vessel-induced NPF events were observed on six of the thirty-one days of the cruise over the SCS (Table 1). There were five daytime events and two nighttime events. The seven NPF events shared some unique features such as the occurrence under ambient RH larger than 70% and dramatic spatiotemporal variations in $N_{<30}$, etc., as presented below. Attempts were made to examine NPF in SCS out of the marginal seas of China, a cruise campaign along the long coast from the Yellow Sea, to the East China Sea to the SCS was conducted in the spring of 2018. Unfortunately, due to weather conditions that were unfavorable for NPF, no NPF event was observed. No NPF event was observed either over the tropic oceanic zones of the NWPO during a cruise campaign in the fall of 2018. Thus, measurements in Hong Kong, adjacent to the SCS, are used to compare and illustrate these unique features (Table 1).

All seven NPF events in SCS occurred under clear weather conditions with ambient RH exceeding 70%. In contrast, the NPF events at the rural site in Hong Kong were all observed at ambient RH below 70% (Man et al., 2015). The continental NPF events were usually observed at low ambient RH (Hamed et al., 2011; Kulmala et al., 2004). Hamed et al. (2011) reported the maximum concentration of sulfuric acid vapor was observed at ambient RH below 60%. NPF events in the continental atmosphere were rarely observed at ambient RH exceeding 70% because of several different seasons, e.g., high ambient RH significantly reduces OH concentrations (Hamed et al., 2011; Kerminen et al. 2018; Kulmala et al., 2004). The daytime NPF events observed in the remote humid marine atmosphere over the SCS might be driven by ambient nucleation independent on ambient RH while nighttime NPF events were also independent on photochemical reactions.

FR has been widely used to characterize NPF events in the literature. The typical FR induced by sulfuric acid nucleation ranges from 0.01 to 10 $cm^{-3}s^{-1}$ in the continental atmospheric boundary layer (Kulmala et al., 2004). We calculated the values of FR during the spring cruise campaign over the SCS and found that they were unrealistically large (as high as 87 $cm^{-3}s^{-1}$ and 112 $cm^{-3}s^{-1}$ on 1 April and 7 April 2017, respectively，the FR was calculated as NMINP/(t_1-t_{01}), t_1 and t_{01} were labeled in Figs. 3b and 3e) that cannot be explained by ambient nucleation of sulfuric acid vapor. However, large FR (10^2-10^4 $cm^{-3}s^{-1}$) is common for reported NPF events induced by iodine compounds in literature (O'Dowd et al., 2002b). However, direct measurements of these iodine compounds in the smaller sized need to confirm this (Yu et al., 2019).

In addition, the NMINP varied from 0.7×10^4 to 9.3×10^4 cm^{-3}, with the mean of $4.5\times10^4\pm3.4\times10^4$ cm^{-3} in five of the seven NPF events (For the event on 31 March, NMINP was calculated after 10:15-10:30). No NMINP was calculated for the other two events due to the lack of measurements in the initial periods. Condensational sink and NMINP are poorly correlated. The mean of NMINP is approximately one order of magnitude large than theoretically estimated and measured NMINP in marine NPF events induced by the oxidation of DMS (Chang et al., 2011; Collins et al., 2017; Dall'Osto et al., 2017; Pirjola et al., 2000) and therefore unlikely induced by the biogenic DMS sources. The mean NMINP in this study over the SCS was also higher than that in the rural coastal areas of Hong Kong (Man et al., 2015) of 1.3×10^4 cm^{-3} and that in the polluted atmosphere over the Yellow Sea and East China Sea of 1.3×10^4 cm^{-3} (Liu et al., 2014). Although no concentrations of sulfuric acid are available for discussion, the concentrations of SO_4^{2-} in particles less than 3.2 μm over the SCS and those in $PM_{2.5}$ in Hong Kong were alternatively used to argue the difference on observed NMINP. The average value was as low as 0.48-1.3 $\mu g/m^3$ during some periods of the campaign over the SCS (not shown), when the particle sampler was not downwind of self-vessel plumes. The average value of SO_4^{2-} during NPF events reached 14.2 $\mu g/m^3$ in Hong Kong as reported by Man et al. (2015). The low concentrations of SO_4^{2-} over the SCS further suggest the background marine atmosphere to be "less polluted", except self-vessel plumes. At such low SO_4^{2-} levels over the SCS, low concentrations of sulfuric acid should be there and unlikely cause high NMINP.

Moreover, Ueda et al. (2016) reported an NMINP of $N_{<30}$ of less than 500 cm^{-3} in the clean marine atmosphere over the North Pacific Ocean, which was approximately two orders of magnitude lower than what we observed over the SCS. However, under the influence of transport of anthropogenic continental air pollutants (see the calculated back trajectories shown in Fig. S2), the NMINP during the NPF events observed in the remote atmosphere over the sub-tropic zone of the NWPO in the spring of 2014 and 2016 ranged from 0.18×10^4 cm^{-3} to 1.8×10^4 cm^{-3}, with the mean of 1.1×10^4 cm^{-3} (Guo et al., 2016; Zhu et al., 2019).

Furthermore, we did not observe the typical "banana-shaped" particle growth in any of the seven NPF events identified over the SCS. The GMD of newly formed particles remained invariant at ~11 nm in these NPF events (Fig. 1a). At the rural site in Hong Kong, the GMD of newly formed particles eventually increased to over 20 nm in all NPF events. However, for the NPF on 16 March 2011 in that study, the GMD of newly formed particles remained invariant at ~10 nm for the initial 40 minutes (bottom left of Fig. 1b in Man et al., 2015).

Overall, these seven events had occurrence conditions with ambient RH>70%, unrealistically large FR and absence of apparent particle growth that are distinctively different from those of NPF events driven by sulfuric acid in coastal and marine atmospheres. These NPF events across SCS were unlikely induced by sea-derived dimethyl sulfide because of their large NMINP. The NMINP even larger than those observed in Hong Kong and the NWPO suggests that the NPF events over the SCS were associated with stronger ambient nucleation.

3.3. Comparison of nighttime and daytime NPF events

On the same day (7 April, Figs. 3d and 3e), the intensity of the nighttime NPF event is clearly weaker than that of the daytime NPF event. The same is generally true for the overall comparison between two nighttime NPF events and five daytime NPF events (Fig. 1a). Solar radiation can initiate photochemical reactions, which would subsequently enhance daytime NPF.

Two nighttime NPF events were observed over the SCS on 2 and 7 April in absence of banana-shaped growth (Figs. 3d-3f and S3d-S3f). We first studied the nighttime NPF event on 7 April because there was no disturbance from self-vessel emissions (Figs. 3d-3f). This event lasted approximately one hour (from 22:30 to 23:40) and occurred over a ~25 km oceanic zone on the basis of the cruise track superimposed in Fig. 3e, with an average $N_{<30}$ of $4.0\times10^3 \pm 2.2\times10^3$ cm^{-3} (green shadow in Fig. 3e). The average $N_{<30}$ was substantially larger than the averages before and after the event ($6.7\times10^2 \pm 2.5\times10^2$ cm^{-3} at 22:00-22:30 and $6.1\times10^2 \pm 67$ cm^{-3} at 23:40-24:00). Note that N_{30-100} decreased by approximately 60% during the NPF events in comparison with from the hourly average value before the event. The FMPS was situated only approximately 20 m distance from the vessel chimney smoke stack. Either a strong signal or no signal from own emission plumes was detected by the FMPS, depending on whether the FMPS was downwind of the stack. The NPF event started with a sharply decreasing wind speed from 6.0 ms^{-1} to 0.5 ms^{-1} and the wind direction changed from west to east (green shadow in Fig. 3f), implying that the stagnant air mass, not self-vessel emission, was related to NPF. Decreasing wind speed is usually caused by descending motions, favoring accumulation of precursors for nucleation. The $N_{<30}$ fluctuated dramatically (Fig. 3e) through the event, which is an indication of high spatiotemporal heterogeneity of new particles.

In contrast, the second nighttime NPF event on 2 April lasted for at least three hours and occurred over at least 60 km oceanic zone on the basis of the vessel cruise track (The bottom of the left column in Fig. 1a and Fig. S3d-S3f), but the starting time was unidentified because of missing data. The NPF event ended at 21:30 when the wind speed suddenly increased from 3.8 ± 0.6 ms^{-1} to 7.8 ± 0.8 ms^{-1} and the wind direction changed from 157±9 °to 217±5°. $N_{<30}$ also dramatically fluctuated during this NPF event when the average $N_{<30}$ was $9.9\times10^3 \pm 5.7\times10^3$ cm^{-3} (Fig. S3e) and sharply decreased to 492 ± 89 cm^{-3} at 21:30-22:00. Unfortunately, a number of spikes in N_{30-100} were observed during the NPF event due to self-vessel emissions (Fig. S3e). When these N_{30-100} spike periods were completely removed, no significant correlation between $N_{<30}$ and N_{30-100} existed, i.e., correlation coefficient of r was as low as 0.05 with P>0.1. In addition, the strongest spike of $N_{<30}$ ($1.3\times10^4 \pm 0.8\times10^4$ cm^{-3}) at 20:53-21:03 occurred concurrently with N_{30-100} to be one order magnitude lower at $1.1\times10^3 \pm 0.3\times10^3$ cm^{-3}. $N_{<30}$ held at $1.4\times10^4 \pm 0.4\times10^4$ cm^{-3} at

20:11-20:31, although $N_{30\text{-}100}$ largely increased by over one order of magnitude and reached $1.6\times10^4\pm1.2\times10^4$ cm^{-3}. The comparison results further indicate that self-vessel plumes had a negligible influence on $N_{<30}$ during the NPF event. Like dramatic fluctuations of $N_{30\text{-}100}$ caused by self-vessel plumes, $N_{<30}$ also dramatically fluctuated, but not simultaneously with $N_{30\text{-}100}$, during the nighttime event. The dramatic fluctuation of $N_{<30}$ implied NPF to be likely driven by locally derived precursors, e.g., reactive iodine compounds proposed in the literature.

The five daytime NPF events were observed on 30, 31 March and 1, 4 and 15 April (Fig. 1a). The longest NPF event was observed on 1 April (Fig. 3a) and the vessel traveled approximately 140 km during this entire NPF period from 10:00 to 16:20 (Fig. 3b). The NPF event apparently occurred regionally, but the temporal profile of $N_{<30}$ implied that the strength of the NPF varied largely in different oceanic zones. The $N_{<30}$ rapidly increased from 663 particles cm^{-3} to 1.3×10^5 cm^{-3} in the initial 26 minutes after 10:00 (green shadow in Fig. 3b) and then dramatically fluctuated around $3.2\times10^4\pm1.7\times10^4$ cm^{-3} at 10:30-13:20 (orange shadow in Fig. 3b). $N_{30\text{-}100}$ was only $2.2\times10^3\pm1.1\times10^3$ cm^{-3} and over one order magnitude lower than $N_{<30}$ in the three hours, indicating the marine atmosphere to be "less polluted". The wind speed narrowly varied around 8.1±0.8 ms^{-1} before 10:00 (green shadow in Fig. 3c), dramatically varied in the next half hour, and then reduced around 4.5±0.7 ms^{-1} at 10:35-12:50 (orange shadow in Fig. 3c). The wind direction turned from 275°±17° before 10:00 to the extreme of 21° and then gradually turned back to 240°±7° at 10:35-12:50. The $N_{<30}$ drastically decreased to $0.7\times10^4\pm0.7\times10^4$ cm^{-3} during 13:20-14:42 (gray shadow in Fig 3b). The new particle signals returned strongly afterwards and the $N_{<30}$ showed another peak of $3.0\times10^4\pm1.6\times10^4$ cm^{-3} at 15:08-15:52 (cyan shadow in Fig. 3b) and then gradually disappeared. Analysis of other daytime NPF events reveals the common feature, i.e., the $N_{<30}$ dramatically fluctuated through the event. However, NPF events induced by sulfuric acid vapor usually exhibited a rapid increase in $N_{<30}$ in the initial one-three hours, followed by a gradual decrease in $N_{<30}$ through the events as reviewed by Kulmala et al. (2004). Formation of sulfuric acid vapor in ambient air is not fast enough and the vapor thereby needs accumulation to some extent for nucleation (Kerminen et al., 2018). It is practically impossible for sulfuric acid vapor repeatedly induces NPF for dozens of times in a few hours (Clarke et al., 1998). Nighttime NPF shares the same feature as daytime NPF.

Moreover, the two strong daytime NPF events were observed under high levels of N_{30-100} on 30 and 31 March (top two in Fig. S3). The NPF event on 31 March was the strongest and was thereby selected to illustrate. During the break of the event (at 10:15-10:30) on that day, $N_{<30}$ and N_{30-100} were as low as $1.3\times10^3\pm1.3\times10^3$ cm^{-3} and $1.1\times10^3\pm98$ cm^{-3}, respectively, indicating the marine atmosphere to be "less polluted". Due to NPF, $N_{<30}$ increased to $5.7\times10^4\pm2.6\times10^4$ before the break (at 08:29-10:14) and after the break (at 10:31-14:39), when N_{30-100} also largely increased to $1.7\times10^4\pm0.9\times10^4$. Two troughs of $N_{<30}$ at 10:39-11:06 and 13:34-13:54 exactly corresponded to two troughs of $N_{<30-100}$ during the NPF event, implying that NPF may reduce with reduced anthropogenic air pollutants' signals. However, $N_{<30}$ was poorly correlated to $N_{<30-100}$ during most of periods of the event. Again, the strength of ambient nucleation depends on the balance of availability of precursors against condensational sink.

3.4. Cause of dramatic variations in $N_{<30}$ during NPF events

Unlike most NPF events observed in continental atmospheres (Kulmala et al., 2013, 2016; Ristovski et al., 2010), the NPF events in the remote marine atmosphere over the SCS show dramatic variations in $N_{<30}$. Wen et al. (2006) also reported dramatic variations in the number concentration of newly formed particles with diameter less than 10 nm in the rural coastal atmosphere at Bodega Bay, California and attributed the NPF events to biogenic activities. The dramatic variations are analyzed below using the CV values as a metric. Meng et al. (2015) reported the CV of $N_{<100}$ to be as low as 0.05±0.02 during banana-shaped NPF events observed in marine atmospheres. The occurrence of NPF largely increased the nucleation mode particle number concentrations and thereby increased the spatial homogeneity of particles in number concentration. In addition to spatial homogeneity of particle number concentration, other factors such as turbulence can affect the CV.

Before analyzing the CV values during the NPF events across the SCS, we first examined the CV values at two typical situations, i.e., in regional plumes and in self-vessel plumes. For example, regional Aitken mode particle signals were detected on 15 April over the SCS (Fig. 2a). The CV for N_{30-100} largely decreased from 0.75±0.09 at one hour immediately before the plume arrival (at 09:30-10:25) to 0.13±0.15 at the initial one hour during the plume arrival (at 10:26-11:25) with an increase in N_{30-100} from 785±179 cm^{-3} to $1.3\times10^4\pm6.3\times10^3$ cm^{-3}. The CV for N_{30-100} further decreased to 0.04 ±0.03 with additionally increasing N_{30-100} at 12:45 to 14:05 on that day. In contrast, self-vessel plumes also caused a large increase in N_{30-100} relative to the clean marine background. For example, N_{30-100} increased largely from $2.2\times10^3\pm0.3\times10^3$ cm^{-3} before the self-vessel plumes at 03:53-04:34 to $1.1\times10^4\pm0.5\times10^4$ cm^{-3} in the self-vessel plumes at 04:35-06:33 (marked with red rectangle in Fig. 2c) on 5 April over the SCS. $N_{<30}$ also increased from 854±55 cm^{-3} to $5.1\times10^3\pm1.9\times10^3$ cm^{-3} in this case, but no increase in $N_{<30}$ occurs in most of self-vessel plumes on that day. The CV values of $N_{<30}$ and N_{30-100} decreased only from 0.97±0.11 to 0.53±0.15 for $N_{<30}$ and only from 0.33±0.06 to 0.27±0.14 for N_{30-100}, with increasing N_{30} and N_{30-100}. The similar result can be obtained for observations at 14:41-17:16 in self-vessel plumes (marked with purple rectangle in Fig. 2c) and at 13:41-14:19 after the self-vessel plumes, i.e., a decrease in CV values from 1.3±0.14 to 0.54±0.15 for $N_{<30}$ and from 0.44±0.08 to 0.27±0.13 for

N_{30-100}. Considering approximately 20 m distance between the FMPS and the self-vessel smokes stack, local turbulence likely overwhelmed advection in determining high-frequency oscillation signals of $N_{<30}$ and N_{30-100} in self-vessel plumes and led to large CV values for $N_{<30}$ and N_{30-100} therein. On the other hand, advection always overwhelms turbulence in regional transport of air pollutants, leading to a much large decrease in CV values with increasing N_{30-100}.

With a large difference in CV values associated with the transport of air pollutants driven by advection and local turbulence in mind, we analyzed the CV values of $N_{<30}$ and N_{30-100} and the CV ratios during the NPF events and before or after the events. Again, we first re-examined these variables during, before or after the NPF events in the spring coastal atmosphere in Hong Kong (Man et al., 2015). Compared to the period before NPF events, based upon the bottom section of Table 1, the $CV_{N<30}$ and ratio of $CV_{N<30}$ to $CV_{N30-100}$ drastically decreased during the NPF events in Hong Kong and increased after the events. The $CV_{N<30}$ were as low as 0.1 during the NPF events therein (bottom section of Table 1). The decreasing extent in CV values was consistent with that for N_{30-100} observed in the regional plume over the SCS on 15 April.

In the SCS, there were seven NPF events and three had no data before the NPF events. On 31 March, there was a break of NPF at 10:15-10:30 and the CV at the break was used for comparison. On 2 April, the CV immediately after the NPF event was used for comparison. The six NPF events can be divided into two general categories compared to the period before or after NPF events. The first category is characterized by reduction in $CV_{N<30}$ and the CV ratio during the events, similar to what was found in self-vessel plumes. There are four NPF events in the first category, i.e., two nighttime events on 2 and 7 April and two daytime events on 31 March and 7 April. However, the values were much larger than those in the regional plume observed over the SCS on 15 April and those during the NPF in Hong Kong, indicating that the transport of newly formed particles may not be dominantly driven by advection. The NPF events may be related to highly localized formation of new particles. In some events, NPF can occasionally be affected by self-vessel plumes as discussed in Section 3.3, indirectly supporting highly localized NPF. On the other hand, NPF events in marine atmospheres were widely proposed to occur aloft in the literature, possibly because of lower ambient temperature or lower condensation sink, and then move to low altitude (Clarke et al., 1998; Meng et al., 2015; Wiedensohler et al., 1996; Sanchez et al., 2018). At ~200 m above the ground level, atmospheric particles formed by iodine compounds have also been observed (O'Dowd et al., 2007). Turbulence always dominates to drive the downward transport of air masses, leading to an oscillation of observed signals in 0.1-10 Hz (Duan et al., 2013). In fact, observed signals of gases and particles in 0.1-10 Hz are widely used to calculate the vertical flux in various atmospheres, i.e., eddy covariance technique. However, the possibility of the turbulence-driven downward transport of newly formed particles in this study was low because 1) wind speeds decreased during the NPF events on 2 and 7 April; 2) the strength of turbulence theoretically decreases with decreasing wind speed.

The second category is characterized by the increases in $CV_{N<30}$ and CV ratios during the events. It includes two daytime events on 1 and 15 April. On 1 April 2017, the $CV_{N<30}$ during the NPF event (0.74±0.34) were significantly larger than those before the event (0.48±0.12), with $P<0.01$. The ratio of $CV_{N<30}$ to $CV_{N30-100}$ during the NPF events (4.2) was also larger than that before the NPF events (3.4). Again, wind speeds largely decreased during the event (Fig. 3c). This increased $N_{<30}$ with the spatial heterogeneity can be attributed to the occurrence of highly heterogeneous NPF in the boundary layer, near sea level, over ~140 km oceanic zone. Its heterogeneity is even larger than those in category 1. On 15 April 2017, when the $CV_{N<30}$ were comparable during the NPF event (0.50±0.14) and before the event (0.57±0.14). The ratio of the CV of $N_{<30}$ to the CV of

N_{30-100} was as large as 11, much larger than that before the NPF event. These results indicated that this NPF event did not increase spatial homogeneities albeit the enhancement of $N_{<30}$. Therefore, we consider this event has similar characteristics and similar mechanism to the one on April 1.

3.5. Weak NPF events over the SCS

We first analyzed one weak NPF event occurring immediately after the strong event (12:45 to 14:05) on 15 April in the marine atmosphere over the SCS (Fig. 2a). The weak new particle signal lasted for approximately 4 hours and gradually disappeared after 18:20 on that day. $N_{<30}$ varied around $1.7\times10^{3}\pm0.4\times10^{3}$ cm^{-3} during the weak event, which were approximately four times less than $N_{<30}$ ($7.9\times10^{3}\pm7.0\times10^{3}$ cm^{3}) during the strong NPF event. However, they were significantly larger than the background values of $0.74\times10^{3}\pm0.35\times10^{3}$ cm^{-3} before the NPF event (at 09:30-10:15) and $0.67\times10^{3}\pm0.26\times10^{3}$ cm^{-3} after the NPF event (at 19:30-21:30) with $P<0.05$. The CV of $N_{<30}$ during the weak NPF event were 0.63±0.17 against 1.25±0.14 before the NPF event and 1.06±0.19 after the NPF event because of increasing spatial homogeneity with increasing $N_{<30}$. During the weak NPF event, no significant correlation between $N_{<30}$ and N_{30-100} with $r=0.37$ and $P>0.1$ and the GMD of nucleation mode particles were almost invariant at 11±0.3 nm. Concentrations of precursors for nucleation in the atmosphere over the travelled oceanic zone after 14:05 may have decreased dramatically, leading to the weak NPF. However, direct measurements of the precursors need to confirm this. We also analyzed meteorological conditions. The reduction in nucleation is not yet to be explained. Overall, the strong NPF event plus the weak NPF event on 15 April occurred over ~30 km oceanic zone of the SCS.

The longest weak NPF event was observed on 27-28 April, but it occurred somewhat intermittently in daytime and nighttime (Fig. 4). Concentrations of precursors over the travelled oceanic zone during the most of time on 27-28 April may allow for the weak nucleation, but it was not the case over the travelled oceanic zone during most of periods from 06:00 to 15:20 on 27 April. For example, $N_{<30}$ varied around $1.1\times10^3\pm0.8\times10^3$ cm^{-3} on 27-28 April, excluding 06:00-15:20 on 27 April. The $N_{<30}$ were significantly larger the background values of $0.58\times10^3\pm0.26\times10^3$ cm^{-3} before the event (at 17:10-24:00 on 26 April). The $N_{<20}$ showed similar trend as $N_{<30}$, and more details were shown in Fig. S4. The weak NPF was clearly enhanced at 15:50-19:40 on 27 April with even larger $N_{<30}$ of $2.0\pm1.2\times10^3$ cm^{-3}. During the longest weak NPF event, no significant correlation between $N_{<30}$ and N_{30-100} with r=0.48 and P>0.1 and the GMD of nucleation mode particles were almost invariant at 11±0.3 nm. The long events further suggested the existence of non self-vessel-induced NPF in the atmosphere over the SCS independent on solar radiation. Overall, either weak NPF events or absence of NPF events generally occurred over the SCS through the campaign. However, strong NPF events occurred sometimes. The SCS is subject to an oligotrophic oceanic zone (Chu et al., 2018), and the sea level anomaly showed upwelling zones to be irregularly distributed in the SCS during the cruise period (Fig. S5). The ocean upwelling carried nutrients from deeper sea water to the surface, which could promote the production of biological precursors from seaweeds (Wen et al., 2006). In addition, the bacteria in oligotrophic marine environments could synthesize CH_3I, which could contribute the source of biological precursors (Amachi et al., 2001; Yokouchi et al., 2012).

3.6. Nucleation mode particles over the NWPO

In October 2018, the averaged particle number concentration distributions over the tropic oceanic zone of the NWPO can be categorized into three periods (Fig. 5). During Period 1 on 9-14 October, nucleation mode particles dominatingly contributed to the total particle number concentration and had the GMD of 25±2 nm. Nucleation mode particles still dominated during

Period 2 on 15-23 October. However, the number concentrations of nucleation mode particles were lower than during Period 1. During Period 3 on 24-29 October, the nucleation, Aitken and accumulation modes were comparable. $N_{<30}$ varied around $1.6\times10^3\pm1.1\times10^3$ during Period 1, $0.5\times10^3\pm1.5\times10^3$ during Period 2 and $3.8\times10^3\pm2.6\times10^3$ during Period 3. On average, N_{30-200} during Period 2 and Period 3 increased by approximately 60% and approximately 300% against Period 1, respectively. The large percentage increases were likely caused by anthropogenic emissions from upwind continents, marine traffics or others. Although nucleation mode particles can be clearly identified through the campaign, NPF events were never observed. Overall, the GMD of nucleation mode particles during Period 1 and 2 were almost invariant, and slightly increased to 27±2 nm during Period 3. No detectable NPF events in the boundary layer, near sea level, through the entire campaign implied that atmospheric nucleation unlikely occurred therein. Sanchez et al. (2018) also reported nucleation mode particles with the GMD of ~25 nm in free troposphere and near sea surface (their Figs. 5a, b) measured by particle sizers on the NASA C-130 aircraft and R/V Atlantis on 20 May 2016 during NAAMES2. They ascribed the nucleation mode particles in the boundary layer, near sea level, to downward transport. Unlike in the SCS, the tropic oceanic zone over the NWPO is conventionally called as "Ocean Desert" (Polovina et al., 2008). Lack of biogenic precursors for nucleation is expected in the boundary layer, near sea level. Recent modeling results proposed that the vertical transport of nucleation mode particles from free troposphere acted as an importance source of these particles in the tropic atmosphere (Williamson et al., 2019). The nucleation mode particles may grow to some extent in different atmospheres, when they transport downward to the boundary layer, near sea level.

3.7. Hindered growth of new particles

In the literature, new particles driven by iodine compounds have been reported to rarely grow larger than 10-20 nm (Ehn et al., 2010; Sipilä et al., 2016). The reported number size distributions of the newly formed particles usually showed negligible or small changes during the NPF period, although the number concentrations varied largely. In this study, the newly formed particles showed no clear growth during NPF events over the SCS. The feature appears to be consistent with NPF driven by iodine compounds. In addition, the regional plume observed on 15 Apr 2017 showed an invariant GMD of preexisting particles at ~50 nm for approximately five hours before the plume disappeared (Fig. 2). This strongly suggests that there was not enough semi-volatile species in the gas phase to promote particle growth through condensation. Kinetic factors such as the gas-particle mass transfer rates for larger 50 nm particles should not be the limiting factor because of their time scales in seconds. For example, Man et al. (2015) observed the growth of newly formed particles encountered a ceiling at 40-50 nm and the GMD was invariant at the ceiling size for a few hours. However, when the product of $HNO_3 \times NH_3$ exceeded the required value (Man et al., 2015), a rapid growth of 40-50 nm particles was observed.

The Kelvin effect term is larger for 10 nm particles than for 50 nm particles. If semi-volatile species cannot thermodynamically support the growth of 50 nm particles, it would be impossible to grow 10 nm particles any larger. No banana-shaped growth was observed during the NPF events over the SCS, as it was apparently restricted by the limited semi-volatile species. In addition, the strongest NPF event on 31 March (Fig. S3) appeared to be sometimes enhanced by anthropogenic combustion air pollutants in particle number concentration. However, no apparent growth of nucleation mode particles was observed either. In a recent literature review, the growth of nucleation mode particles can be driven by highly oxidized low volatile biogenic organic vapor associated with emissions from coniferous forests (Kerminen et al., 2018). However, coniferous forests in tropic marine environments are not expected.

As a comparison, the clear banana-shaped growth observed in Hong Kong implied that the concentrations of semi-volatile species in the coastal atmosphere of the SCS were generally larger than the threshold for condensation on newly formed particles to occur. However, the lack of apparent growth in the initial 40 minutes of one NPF event in Hong Kong (the NPF event shown in the left bottom of Fig. 1b) showed that it might also be limited by the abundance of semi-volatiles (Man et al., 2015). In addition, the banana-shaped growth of newly formed particles was also observed in the sub-tropic atmosphere over the NWPO. The 24-hr back trajectories during those NPF events showed that air masses travelled over the continent (Fig. S2). Notably, the apparent growth of newly formed particles and preexisting particles were simultaneously observed on 25 March 2016 (Fig. 1b). The growth rate of preexisting particles (36.7 nm/h) was larger than that of newly formed particles (4.9 nm/h) during the NPF event in 2016 over the NWPO (Fig. 1b). Semi-volatile species with higher volatility may preferably condense on preexisting particles with larger size over newly formed particles because of the stronger Kelvin effect of the smaller particles (Burkart et al., 2017). In contrast, no apparent growth of newly formed particles and preexisting particles were observed across the SCS (Fig. 1a).

Based on the above comparison, it can be reckoned that the atmosphere over the SCS during the observational period lacked key precursors from the continent to support the growth of newly formed particles. However, the 24-h back trajectories during the NPF events over the SCS showed that air masses sometimes came from the remote area in the Philippines. More studies are needed to explore those key precursors.

4. Conclusion

In this study, two strong nighttime and five strong daytime NPF events as well as several weak NPF events were identified in the remote marine atmosphere during a cruise campaign across the SCS from 29 March to 2 May 2017. The cruise track during the strong NPF events identified that they occurred over a region from approximately 2 km to over 140 km. The NMINP of NPF events were as high as 0.7-9.3×10^4 cm^{-3}, with an average of 4.5×10^4 cm^{-3}, implying large variations in concentration of aerosol precursors in the marine atmosphere. Moreover, dramatic high-frequency variations in $N_{<30}$ during the NPF events strongly suggest that they are affected by the turbulence. The possibility of strong turbulence-driven downward transport of newly formed particles was low, but we had no measurements aloft to confirm this. Our comprehensive analyses indicate that the NPF events were not likely originate from sulfuric acid vapor. Moreover, our comparison analyses suggest that the lack of banana-shaped growth might be due to limited abundance of key precursors for the growth of newly formed particles.

In contrast, NPF events were surprisingly never observed over the tropic zone of the NWPO. However, the nucleation particle mode with GMD mostly at 25±2 nm was clearly observed and sometimes even dominated over other particle modes during the cruise. Combining the absence of NPF events and observed GMD of nucleation mode particles, we conclude the nucleation mode particles are probably not generated in the boundary layer, near sea level. Alternatively, they might be due to the downward transport from aloft.

Overall, sources and formation mechanisms of nucleation mode particles in tropic marine atmospheres apparently highly varied. To better understand their climate impacts of the nucleation mode particles, more observations at least in different seasons, are needed.

Declaration of competing interests

The authors declare that they have no known competing financial interests or personal relationships that could have appeared to influence the work reported in this paper.

Acknowledgement

This research is supported by the National Key Research and Development Program in China (grant no. 2016YFC0200504) and the Natural Science Foundation of China (grant no. 41576118).

References

Allan, J. D., Williams, P. I., Najera, J., Whitehead, J. D., Flynn, M. J., Taylor, J. W., Liu, D., Darbyshire, E., Carpenter, L. J., Chance, R., Andrews, S. J., Hackenberg, S. C. and McFiggans, G., 2015. Iodine observed in new particle formation events in the Arctic atmosphere during ACCACIA. Atmos. Chem. Phys., 15(10), 5599–5609, http://doi.rog/10.5194/acp-15-5599-2015.

Amachi, S., Kamagata, Y. and Kanagawa, T., 2001. Bacteria Mediate Methylation of Iodine in Marine and Terrestrial Environments Bacteria Mediate Methylation of Iodine in Marine and Terrestrial Environments. Appl. Environ. Microbiol., 67(6), 2718–2722, http://doi.rog/10.1128/AEM.67.6.2718.

Burkart, J., Hodshire, A. L., Mungall, E. L., Pierce, J. R., Collins, D. B., Ladino, L. A., Lee, A. K. Y., Irish, V., Wentzell, J. J. B., Liggio, J., Papakyriakou, T., Murphy, J. and Abbatt, J., 2017. Organic Condensation and Particle Growth to CCN Sizes in the Summertime Marine Arctic Is Driven by Materials More Semivolatile Than at Continental Sites. Geophys. Res. Lett., 44(20), 10,725-10,734, http://doi.rog/10.1002/2017GL075671.

Chang, R. Y. W., Sjostedt, S. J., Pierce, J. R., Papakyriakou, T. N., Scarratt, M. G., Michaud, S., Levasseur, M., Leaitch, W. R. and Abbatt, J. P. D.: Relating atmospheric and oceanic DMS levels to particle nucleation events in the Canadian Arctic. J. Geophys. Res. Atmos., 116(21), 1–10, http://doi.rog/10.1029/2011JD015926, 2011.

Chu, B., Kerminen, V.-M., Bianchi, F., Yan, C., Petäjä, T. and Kulmala, M., 2019. Atmospheric new particle formation in China. Atmos. Chem. Phys., 19(1), 115–138, http://doi.rog/10.5194/acp-19-115-2019.

Chu, Q., Liu, Y., Shi, J., Zhang, C., Gong, X., Yao, X., Guo, X. and Gao, H., 2018. Promotion Effect of Asian Dust on Phytoplankton Growth and Potential Dissolved Organic Phosphorus Utilization in the South China Sea. J. Geophys. Res. Biogeosciences, 123(3), 1101–1116, http://doi.rog/10.1002/2017JG004088.

Clarke, A. D., Davis, D., Kapustin, V. N., Eisele, F., Chen, G., Paluch, I., Lenschow, D., Bandy, A. R., Thornton, D., Moore, K., Mauldin, L., Tanner, D., Litchy, M., Carroll, M. A., Collins, J. and Albercook, G., 1998. Particle nucleation in the tropical boundary layer and its coupling to marine sulfur sources. Science, 282(5386), 89–92, http://doi.rog/10.1126/science.282.5386.89.

Collins, D. B., Burkart, J., Chang, R. Y.-W., Lizotte, M., Boivin-Rioux, A., Blais, M., Mungall, E. L., Boyer, M., Irish, V. E., Massé, G., Kunkel, D., Tremblay, J.-É., Papakyriakou, T., Bertram, A. K., Bozem, H., Gosselin, M., Levasseur, M. and Abbatt, J. P. D., 2017. Frequent ultrafine particle formation and growth in the Canadian Arctic marine and coastal environments. Atmos. Chem. Phys., 17, 13119–13138, http://doi.rog/org/10.5194/acp-17-13119-2017.

Croft, B., Martin, R. V., Richard Leaitch, W., Tunved, P., Breider, T. J., D'Andrea, S. D. and Pierce, J. R., 2016. Processes controlling the annual cycle of Arctic aerosol number and size distributions. Atmos. Chem. Phys., 16(6), 3665–3682, http://doi.rog/10.5194/acp-16-3665-2016.

Dall'Osto, M., Beddows, D. C. S., Tunved, P., Krejci, R., Ström, J., Hansson, H. C., Yoon, Y. J., Park, K. T., Becagli, S., Udisti, R., Onasch, T., Ódowd, C. D., Simó, R. and Harrison, R. M., 2017. Arctic sea ice melt leads to atmospheric new particle formation. Sci. Rep., 7(1), 1–10, http://doi.rog/10.1038/s41598-017-03328-1.

Deng, Y., Gao, T., Gao, H., Yao, X. and Xie, L., 2014. Regional precipitation variability in East Asia related to climate and environmental factors during 1979-2012. Sci. Rep., 4, 1–13, http://doi.rog/10.1038/srep05693.

Duan, Z., Gao, H., Gao, Z., Wang, R., Xue, Y. and Yao, X., 2013. An Approach to Minimizing Artifacts Caused by Cross-Sensitivity in the Determination of Air-Sea CO_2 Flux Using the Eddy-Covariance Technique. Boundary-Layer Meteorol., 148(1), 227–239, http://doi.rog/10.1007/s10546-013-9814-1.

Ehn, M., Vuollekoski, H., Petäjä, T., Kerminen, V.-M., Vana, M., Aalto, P., de Leeuw, G., Ceburnis, D., Dupuy, R., O'Dowd, C. D. and Kulmala, M., 2010. Growth rates during coastal and marine new particle formation in western Ireland. J. Geophys. Res., 115(D18), D18218, http://doi.rog/10.1029/2010JD014292.

English, J. M., Toon, O. B., Mills, M. J. and Yu, F., 2011. Corrigendum to "Microphysical simulations of new particle formation in the upper troposphere and lower stratosphere". Atmos. Chem. Phys., 11, 9303–9322, http://doi.rog/ 10.5194/acp-11-9303-2011.

Gong, Y., Hu, M., Cheng, Y., Su, H., Yue, D., Liu, F., Wiedensohler, A., Wang, Z., Kalesse, H., Liu, S., Wu, Z., Xiao, K., Mi, P. and Zhang, Y., 2010. Competition of coagulation sink and source rate: New particle formation in the Pearl River Delta of China. Atmos. Environ., 44(27), 3278–3285, http://doi.rog/10.1016/j.atmosenv.2010.05.049.

Guo, H., Wang, D. W., Cheung, K., Ling, Z. H., Chan, C. K. and Yao, X. H., 2012. Observation of aerosol size distribution and new particle formation at a mountain site in subtropical Hong Kong. Atmos. Chem. Phys., 12(20), 9923–9939, http://doi.rog/10.5194/acp-12-9923-2012.

Guo, T., Li, K., Zhu, Y., Gao, H. and Yao, X., 2016. Concentration and size distribution of particulate oxalate in marine and coastal atmospheres – Implication for the increased importance of oxalate in nanometer atmospheric particles. Atmos. Environ., 142, 19–31, http://doi.rog/10.1016/j.atmosenv.2016.07.026.

Hamed, A., Korhonen, H., Sihto, S. L., Joutsensaari, J., Jrvinen, H., Petäjä, T., Arnold, F., Nieminen, T., Kulmala, M., Smith, J. N., Lehtinen, K. E. J. and Laaksonen, A., 2011. The role of relative humidity in continental new particle formation. J. Geophys. Res. Atmos., 116(3), http://doi.rog/10.1029/2010JD014186.

Huang, R.-J. J., Seitz, K., Neary, T., O'Dowd, C. D., Platt, U., Hoffmann, T., O'Dowd, C. D., Platt, U. and Hoffmann, T.. 2010: Observations of high concentrations of I 2 and IO in coastal air supporting iodine-oxide driven coastal new particle formation. Geophys. Res. Lett., 37, L03830, http://doi.rog/10.1029/2009GL041467.

Hu, Q., Yu, P., Zhu, Y., Li, K., Gao, H. and Yao, X., 2015. Concentration, Size Distribution, and Formation of Trimethylaminium and Dimethylaminium Ions in Atmospheric Particles over Marginal Seas of China. J. Atmos. Sci., 72(9), 3487–3498, http://doi.rog/10.1175/JAS-D-14-0393.1.

John, J.G., Stock, C.A., Dunne, J.P., 2015. A more productive, but different, ocean after mitigation. Geophys. Res. Lett. 42, 9836–9845. http://doi.org/10.1002/2015GL066160.

John, V. O., Allan, R. P. and Soden, B. J., 2009. How robust are observed and simulated precipitation responses to tropical ocean warming? Geophys. Res. Lett., 36(14), 1–5, http://doi.rog/10.1029/2009GL038276.

Kerminen, V. M., Paramonov, M., Anttila, T., Riipinen, I., Fountoukis, C., Korhonen, H., Asmi, E., Laakso, L., Lihavainen, H., Swietlicki, E., Svenningsson, B., Asmi, A., Pandis, S. N., Kulmala, M. and Petäjä, T., 2012. Cloud condensation nuclei production associated with atmospheric nucleation: A synthesis based on existing literature and new results. Atmos. Chem. Phys., 12(24), 12037–12059, http://doi.rog/10.5194/acp-12-12037-2012.

Kerminen, V. M., Chen, X., Vakkari, V., Petäjä, T., Kulmala, M. and Bianchi, F., 2018. Atmospheric new particle formation and growth: Review of field observations. Environ. Res. Lett., 13(10), http://doi.rog/10.1088/1748-9326/aadf3c.

Kulmala, M. and Kerminen, V. M., 2008. On the formation and growth of atmospheric nanoparticles. Atmos. Res., 90(2–4), 132–150, http://doi.rog/10.1016/j.atmosres.2008.01.005.

Kulmala, M., Vehkamäki, H., Petäjä, T., Dal Maso, M., Lauri, A., Kerminen, V. M., Birmili, W. and McMurry, P. H., 2004. Formation and growth rates of ultrafine atmospheric particles: A review of observations. J. Aerosol Sci., 35(2), 143–176, http://doi.rog/10.1016/j.jaerosci.2003.10.003.

Kulmala, M., Kontkanen, J., Junninen, H., Lehtipalo, K., Manninen, H. E., Nieminen, T., Petäjä, T., Sipilä, M., Schobesberger, S., Rantala, P., Franchin, A., Jokinen, T., Järvinen, E., Äijälä, M., Kangasluoma, J., Hakala, J., Aalto, P. P., Paasonen, P., Mikkilä, J., Vanhanen, J., Aalto, J., Hakola, H., Makkonen, U., Ruuskanen, T., Mauldin, R. L., Duplissy, J., Vehkamäki, H., Bäck, J., Kortelainen, A., Riipinen, I., Kurtén, T., Johnston, M. V, Smith, J. N., Ehn, M., Mentel, T. F., Lehtinen, K. E. J., Laaksonen, A., Kerminen, V.-M., Worsnop, D. R., Hanna, E., Nieminen, T., Petäjä, T., Sipilä, M., Schobesberger, S., Rantala, P., Franchin, A., Jokinen, T., Järvinen, E., Äijälä, M., Hakala, J., Aalto, P. P., Paasonen, P., Mikkilä, J., Aalto, J., Hakola, H., Makkonen, U., Ruuskanen, T., Roy, L., Iii, M., Duplissy, J., Vehkamäki, H., Bäck, J., Kortelainen, A., Kurtén, T., Johnston, M. V, Smith, J. N., Ehn, M., Thomas, F., Lehtinen, K. E. J., Laaksonen, A., Kerminen, V.-M. and Worsnop, D. R., 2013. Direct Observations of Atmospheric Aerosol Nucleation. Science, 339(6122), 943–946, http://doi.rog/10.1126/science.1227385.

Kulmala, M., Petäjä, T., Nieminen, T., Sipilä, M., E Manninen, H., Lehtipalo, K., Dal Maso, M., Aalto, P., Junninen, H., Paasonen, P., Riipinen, I., E J Lehtinen, K., Laaksonen, A. and Kerminen, V.-M., 2012. Measurement of the nucleation of atmospheric aerosol particles. Nature Protocols, 7, 1651–1667 http://doi.rog/10.1038/nprot.2012.091.

Kulmala, M., Petäjä, T., Kerminen, V.-M., Kujansuu, J., Ruuskanen, T., Ding, A., Nie, W., Hu, M., Wang, Z., Wu, Z., Wang, L. and Worsnop, D., 2016. On secondary new particle formation in China. Front. Environ. Sci. Eng., 10 (5), 8, http://doi.rog/10.1007/s11783-016-0850-1.

Leaitch, W. R., Sharma, S., Huang, L., Toom-Sauntry, D., Chivulescu, A., Macdonald, A. M., Von Salzen, K., Pierce, J. R., Bertram, A. K., Schroder, J. C., Shantz, N. C., Chang, R. Y. W. Y.-W. and Norman, A.-L. L., 2013. Dimethyl sulfide control of the clean summertime Arctic aerosol and cloud. Elementa, 1, 1–12, http://doi.rog/10.12952/journal.elementa.000017.

Lauvset, K.S., Tjiputra, J., Muri, H., 2017. Climate engineering and the ocean: Effects on biogeochemistry and primary production. Biogeosciences 14, 5675–5691. http://doi.org/10.5194/bg-14-5675-2017.

Li, K., Zhu, Y., Gao, H. and Yao, X., 2015. A comparative study of cloud condensation nuclei measured between non-heating and heating periods at a suburb site of Qingdao in the North China. Atmos. Environ., 112, 40–53, http://doi.rog/10.1016/j.atmosenv.2015.04.024.

Liu, S., Hu, M., Wu, Z., Wehner, B., Wiedensohler, A. and Cheng, Y., 2008. Aerosol number size distribution and new particle formation at a rural/coastal site in Pearl River Delta (PRD) of China. Atmos. Environ., 42(25), 6275–6283, http://doi.rog/10.1016/j.atmosenv.2008.01.063.

Liu, X. H., Zhu, Y. J., Zheng, M., Gao, H. W. and Yao, X. H., 2014. Production and growth of new particles during two cruise campaigns in the marginal seas of China. Atmos. Chem. Phys., 14(15), 7941–7951, http://doi.rog/10.5194/acp-14-7941-2014.

Man, H., Zhu, Y., Ji, F., Yao, X., Lau, N. T., Li, Y., Lee, B. P. and Chan, C. K., 2015. Comparison of Daytime and Nighttime New Particle Growth at the HKUST Supersite in Hong Kong. Environ. Sci. Technol., 49(12), 7170–7178, http://doi.rog/10.1021/acs.est.5b02143.

McFiggans, G., Coe, H., Burgess, R., Allan, J., Cubison, M., Alfarra, M. R., Saunders, R., Saiz-Lopez, A., Plane, J. M. C., Wevill, D., Carpenter, L., Rickard, A. R. and Monks, P. S., 2004. Direct evidence for coastal iodine particles from Laminaria macroalgae – linkage to emissions of molecular iodine. Atmos. Chem. Phys., 4(3), 701–713, http://doi.rog/10.5194/acp-4-701-2004.

McFiggans, G., Bale, C. S. E., Ball, S. M., Beames, J. M., Bloss, W. J., Carpenter, L. J., Dorsey, J., Dunk, R., Flynn, M. J., Furneaux, K. L., Gallagher, M. W., Heard, D. E., Hollingsworth, A. M., Hornsby, K., Ingham, T., Jones, C. E., Jones, R. L., Kramer, L. J., Langridge, J. M., Leblanc, C., LeCrane, J. P., Lee, J. D., Leigh, R. J., Longley, I., Mahajan, A. S., Monks, P. S., Oetjen, H., Orr-Ewing, A. J., Plane, J. M. C., Potin, P., Shillings, A. J. L., Thomas, F., Von Glasow, R., Wada, R., Whalley, L. K. and Whitehead, J. D., 2010. Iodine-mediated coastal particle formation: An overview of the Reactive Halogens in the Marine boundary layer (RHaMBLe) Roscoff coastal study. Atmos. Chem. Phys., 10(6), 2975–2999, http://doi.rog/10.5194/acp-10-2975-2010.

Meng, H., Zhu, Y., Evans, G. J. and Yao, X., 2015. An approach to investigate new particle formation in the vertical direction on the basis of high time-resolution measurements at ground level and sea level. Atmos. Environ., 102, 366–375, http://doi.rog/10.1016/j.atmosenv.2014.12.016.

Minguillón, M., Brines, M., Perez, N., Reche, C., Pandolfi, M., Fonseca, A., Amato, F., Alastuey, A., Lyasota, A., Codina, B., Lee, H.-K., Eun, H.-R., Ahn, K.-H. and Querol, X., 2015. New particle formation at ground level and in the vertical column over the Barcelona area. Atmos. Res., 164-165, 118-130, http://doi.rog/10.1016/j.atmosres.2015.05.003.

Nieminen, T., Kerminen, V.-M., Petäjä, T., Aalto, P. P., Arshinov, M., Asmi, E., Baltensperger, U., Beddows, D. C. S., Beukes, J. P., Collins, D., Ding, A., Harrison, R. M., Henzing, B., Hooda, R., Hu, M., Hõrrak, U., Kivekäs, N., Komsaare, K., Krejci, R., Kristensson, A., Laakso, L., Laaksonen, A., Leaitch, W. R., Lihavainen, H., Mihalopoulos, N., Németh, Z., Nie, W., O 'dowd, C., Salma, I., Sellegri, K., Svenningsson, B., Swietlicki, E., Tunved, P., Ulevicius, V., Vakkari, V., Vana, M., Wiedensohler, A., Wu, Z., Virtanen, A. and Kulmala, M., 2018. Global analysis of continental boundary layer new particle formation based on long-term measurements. Atmos. Chem. Phys. 18, 14737–14756, http://doi.rog/10.5194/acp-18-14737-2018.

O'Dowd, C. D., Monahan, C. and Dall'Osto, M., 2010. On the occurrence of open ocean particle production and growth events. Geophys. Res. Lett., 37(19), 2–6, http://doi.rog/10.1029/2010GL044679.

O 'dowd, C. D., Hämeri, K., Mäkelä, J. M., Pirjola, L., Kulmala, M., Gerard Jennings, S., Berresheim, H., Hansson, H.-C. C., de Leeuw, G., J Kunz, G., G Allen, A., Hewitt, C. N., Jackson, A., Viisanen, Y., Hoffmann, T., O'Dowd, C. D., Hämeri, K., Mäkelä, J. M., Pirjola, L., Kulmala, M., Jennings, S. G., Berresheim, H., Hansson, H.-C. C., de Leeuw, G., Kunz, G. J., Allen, A. G., Hewitt, C. N., Jackson, A., Viisanen, Y. and Hoffmann, T., 2002a. A dedicated study of New Particle Formation and Fate in the Coastal Environment (PARFORCE): Overview of objectives and achievements. J. Geophys. Res. Atmos., 107(8108), http://doi.rog/10.1029/2001JD000555.

O'dowd, C. D., Jimenez, J. L., Bahreini, R., Flagan, R. C., Seinfeld, J. H., Hämerl, K., Pirjola, L., Kulmala, M. and Hoffmann, T., 2002b. Marine aerosol formation from biogenic iodine emissions. Nature, 417(6889), 632–636, http://doi.rog/10.1038/nature00775.

O'Dowd, C. D., Yoon, Y. J., Junkerman, W., Aalto, P., Kulmala, M., Lihavainen, H. and Viisanen, Y., 2007. Airborne measurements of nucleation mode particles I: Coastal nucleation and growth rates. Atmos. Chem. Phys., 7(6), 1491–1501, http://doi.rog/10.5194/acp-7-1491-2007.

Polovina, J. J., Howell, E. A. and Abecassis, M., 2008. Ocean's least productive waters are expanding. Geophys. Res. Lett., 35(3), 2–6, http://doi.rog/10.1029/2007GL031745.

Quinn, P. K. and Bates, T. S., 2011. The case against climate regulation via oceanic phytoplankton sulphur emissions. Nature, 480(7375), 51–56, http://doi.rog/10.1038/nature10580.

Rose, C., Zha, Q., Dada, L., Yan, C., Lehtipalo, K., Junninen, H., Mazon, S.B., Jokinen, T., Sarnela, N., Sipilä, M., Petäjä, T., Kerminen, V.-M., Bianchi, F. and Kulmala, M. (2018) Observations of biogenic ion-induced cluster formation in the atmosphere, Sci. Adv. 4: eaar5218.

Ristovski, Z. D., Suni, T., Kulmala, M., Boy, M., Meyer, N. K., Duplissy, J., Turnipseed, A., Morawska, L. and Baltensperger, U., 2010. The role of sulphates and organic vapours in growth of newly formed particles in a eucalypt forest. Atmos. Chem. Phys., 10(6), 2919–2926, http://doi.rog/10.5194/acp-10-2919-2010.

Sanchez, K. J., Chen, C. L., Russell, L. M., Betha, R., Liu, J., Price, D. J., Massoli, P., Ziemba, L. D., Crosbie, E. C., Moore, R. H., Müller, M., Schiller, S. A., Wisthaler, A., Lee, A. K. Y., Quinn, P. K., Bates, T. S., Porter, J., Bell, T. G., Saltzman, E. S., Vaillancourt, R. D. and Behrenfeld, M. J., 2018. Substantial Seasonal Contribution of Observed Biogenic Sulfate Particles to Cloud Condensation Nuclei. Sci. Rep., 8(1), 1–14, http://doi.rog/10.1038/s41598-018-21590-9.

Sellegri, K., Pey, J., Rose, C., Culot, A., DeWitt, H. L., Mas, S., Schwier, A. N., Temime-Roussel, B., Charriere, B., Saiz-Lopez, A., Mahajan, A. S., Parin, D., Kukui, A., Sempere, R., D'Anna, B. and Marchand, N., 2016. Evidence of atmospheric nanoparticle formation from emissions of marine microorganisms. Geophys. Res. Lett., 43(12), 6596–6603, http://doi.rog/10.1002/2016GL069389.

Sipilä, M., Sarnela, N., Jokinen, T., Henschel, H., Junninen, H., Kontkanen, J., Richters, S., Kangasluoma, J., Franchin, A., Peräkylä, O., Rissanen, M. P., Ehn, M., Vehkamäki, H., Kurten, T., Berndt, T., Petäjä, T., Worsnop, D., Ceburnis, D., Kerminen, V. M., Kulmala, M. and O'Dowd, C., 2016. Molecular-scale evidence of aerosol particle formation via sequential addition of HIO_3. Nature, 537(7621), 532–534, http://doi.rog/10.1038/nature19314.

Ueda, S., Miura, K., Kawata, R., Furutani, H., Uematsu, M., Omori, Y. and Tanimoto, H., 2016. Number–size distribution of aerosol particles and new particle formation events in tropical and subtropical Pacific Oceans. Atmos. Environ., 142, 324–339, http://doi.rog/10.1016/j.atmosenv.2016.07.055.

Venzac, H., Laj, P. and Sellegri, K., 2008. High frequency new particle formation in the Himalayas. Pnas, 105, 15666–15671, http://doi.rog/10.1073/pnas.0801355105.

Wang, S. X., Zhao, B., Cai, S. Y., Klimont, Z., Nielsen, C. P., Morikawa, T., Woo, J. H., Kim, Y., Fu, X., Xu, J. Y., Hao, J. M. and He, K. B., 2014. Emission trends and mitigation options for air pollutants in East Asia. Atmos. Chem. Phys., 14(13), 6571–6603, http://doi.rog/10.5194/acp-14-6571-2014.

Weber, R. J., McMurry, P.H. , Mauldin, R. L., Tanner, D. J., Eisele, F. L., Clarke, A. D. and. Kapustin, V. N., 1999. New Particle Formation in the Remote Troposphere: A Comparison of Observations at Various Sites. Geophys. Res. Lett., 26(3), 307–310, http://doi.rog/10.1029/1998GL900308.

Wen, J., Zhao, Y. and Wexler, A. S., 2006. Marine particle nucleation: Observation at Bodega Bay, California. J. Geophys. Res. Atmos., 111(8), 1–11, http://doi.rog/10.1029/2005JD006210.

Whitby, K. T., 1978. The physical characteristics of sulfur aerosols. Atmos. Environ., 12(1–3), 135–159, http://doi.rog/10.1016/0004-6981(78)90196-8.

Wiedensohler, A., Covert, D. S., Swietlicki, E., Aalto, P., Heintzenberg, J. and Leck, C., 1996. Occurrence of an ultrafine particle mode less than 20 nm in diameter in the marine boundary layer during Arctic summer and autumn. Tellus, Ser. B Chem. Phys. Meteorol., 48(2), 213–222, http://doi.rog/10.3402/tellusb.v48i2.15887.

Williamson, C. J., Kupc, A., Axisa, D., Bilsback, K. R., Bui, T., Campuzano-Jost, P., Dollner, M., Froyd, K. D., Hodshire, A. L. and Jimenez, J. L., 2019. A large source of cloud condensation nuclei from new particle formation in the tropics. Nature, 574(7778), 399–403, http://doi.rog/10.1038/s41586-019-1638-9.

Xie, H., Feng, L., Hu, Q., Zhu, Y., Gao, H., Gao, Y. and Yao, X., 2018. Concentration and size distribution of water-extracted dimethylaminium and trimethylaminium in atmospheric particles during nine campaigns - Implications for sources, phase states and formation pathways. Sci. Total Environ., 631–632, 130–141, http://doi.rog/10.1016/j.scitotenv.2018.02.303.

Xie, Y., Ding, A., Nie, W., Mao, H., Qi, X., Huang, X., Xu, Z., Kerminen, V. M., Petäjä, T., Chi, X., Virkkula, A., Boy, M., Xue, L., Guo, J., Sun, J., Yang, X., Kulmala, M. and Fu, C., 2015. Enhanced sulfate formation by nitrogen dioxide: Implications from in-situ observations at the SORPES station. J. Geophys. Res., 120(24), 12,679-12,694, http://doi.rog/10.1002/2015JD023607.

Yao, X. and Zhang, L., 2019. Causes of Large Increases in Atmospheric Ammonia in the Last Decade across North America. ACS Omega, 4, 22133–22142, http://doi.rog/10.1021/acsomega.9b03284.

Yao, X., Lau, N. T., Fang, M. and Chan, C. K., 2005. Real-time observation of the transformation of ultrafine atmospheric particle modes. Aerosol Sci. Technol., 39(9), 831–841, http://doi.rog/10.1080/02786820500295248.

Yao, X., Choi, M. Y., Lau, N. T., Lau, A. P. S., Chan, C. K. and Fang, M., 2010. Growth and shrinkage of new particles in the atmosphere in Hong Kong. Aerosol Sci. Technol., 44(8), 639–650, http://doi.rog/10.1080/02786826.2010.482576.

Yokouchi, Y., Nojiri, Y., Toom-Sauntry, D., Fraser, P., Inuzuka, Y., Tanimoto, H., Nara, H., Murakami, R. and Mukai, H., 2012. Long-term variation of atmospheric methyl iodide and its link to global environmental change. Geophys. Res. Lett., 39(23), 1–5, http://doi.rog/10.1029/2012GL053695.

Yu, F. and Luo, G., 2009. Simulation of particle size distribution with a global aerosol model: Contribution of nucleation to aerosol and CCN number concentrations. Atmos. Chem. Phys., 9(20), 7691–7710, http://doi.rog/10.5194/acp-9-7691-2009.

Yu, F., Luo, G., Pryor, S. C., Pillai, P. R., Lee, S. H., Ortega, J., Schwab, J. J., Hallar, A. G., Leaitch, W. R., Aneja, V. P., Smith, J. N., Walker, J. T., Hogrefe, O. and Demerjian, K. L., 2015. Spring and summer contrast in new particle formation over nine forest areas in North America. Atmos. Chem. Phys., 15(24), 13993–14003, http://doi.rog/10.5194/acp-15-13993-2015.

Yu, H., Ren, L., Huang, X., Xie, M., He, J. and Xiao, H., 2019. Iodine speciation and size distribution in ambient aerosols at a coastal new particle formation hotspot in China. Atmos. Chem. Phys., 19(6), 4025–4039, http://doi.rog/10.5194/acp-19-4025-2019.

Zhang, R., Suh, I., Zhao, J., Zhang, D., Fortner, E. C., Tie, X., Molina, L. T. and Molina, M. J., 2004. Formation Enhanced by Organic Acids. Science, 304(2000), 2000–2003, http://doi.rog/10.1126/science.1095139.

Zhang, R., Khalizov, A., Wang, L., Hu, M. and Xu, W., 2012. Nucleation and growth of nanoparticles in the atmosphere. Chem. Rev., 112, 1957–2011, http://doi.rog/10.1021/cr2001756.

Zhu, Y., Yan, C., Zhang, R., Wang, Z., Zheng, M., Gao, H., Gao, Y. and Yao, X., 2017. Simultaneous measurements of new particle formation in 1-second time resolution at a street site and a rooftop site. Atmos. Chem. Phys., 17, 9469–9484 , https://doi.org/10.5194/acp-17-9469-2017.

Zhu, Y., Li, K., Shen, Y., Gao, Y., Liu, X., Yu, Y., Gao, H. and Yao, X., 2019. New particle formation in the marine atmosphere during seven cruise campaigns. Atmos. Chem. Phys., 19(1), 89–113, http://doi.rog/10.5194/acp-19-89-2019.

Zimmerman, N., Jeong, C. H., Wang, J. M., Ramos, M., Wallace, J. S. and Evans, G. J., 2015. A source-independent empirical correction procedure for the fast mobility and engine exhaust particle sizers. Atmos. Environ., 100, 178–184, http://doi.rog/10.1016/j.atmosenv.2014.10.054.

Figure Captions

Fig. 1. NPF events observed in the atmosphere across SCS, NWPO and in Hong Kong. ((a) NPF events observed in the atmosphere across SCS, the blue bars represent the number concentration of the 5.6-30 nm particles ($N_{<30}$), the red line represents the cruise track across SCS during the period of 29 March to 2 May 2017; (b) NPF events observed in the atmosphere across NWPO in comparison with NPF in Hong Kong, the blue bars are defined as same as those across SCS, the red and gray lines represent the cruise track across NWPO in 2014 and 2016 individually.

Fig. 2. NPF event observed on 15 April 2017 (left column) and plume observed on 5 April 2017 (right column) in the atmosphere across SCS. ((a), (c) contour plot of particles number concentration (dN/d log D_p); (b), (d) time series of $N_{<30}$ and $N_{30\text{-}100}$; (e) the vessel track at 10:25-16:45 superimposed in (b) and NPF was observed at the track of red line; the direction of the dotted arrow represents the predominant wind direction during NPF events.

Fig. 3. NPF event observed on 1 (left column) and 7 April 2017 (right column) ((a), (d) contour plots particles number concentration (dN/d log D_p); (b), (e) time series of $N_{<30}$ and $N_{30\text{-}100}$; (c), (f) time series of wind direction and speed; The vessel track superimposed in (b) and (d), and red line is the track where NPF was observed; the direction of the dotted arrow represents the predominant wind direction during NPF events.

Fig. 4. Weak NPF events observed on 27-28 Apr. ((a) contour plots particles number concentration (dN/d log D_p); (b) The vessel track during 27-28 Apr and the direction of the dotted arrow represents the predominant wind direction during NPF events; (c) time series of $N_{<30}$ and $N_{30\text{-}100}$; (d) time series of wind direction and speed.

Fig. 5. (a), (b), (c) the vessel tracks during period 1 (09-14 Oct), period 2 (15-23 Oct) and period 3 (24-29 Oct) across NWPO in 2018; (d), (e), (f) particle size distribution during period 1, 2 and 3 respectively; (g) contour plots particles number concentration (dN/d log D_p) without self-vessel plume during 09-29 Oct across NWPO in 2018.

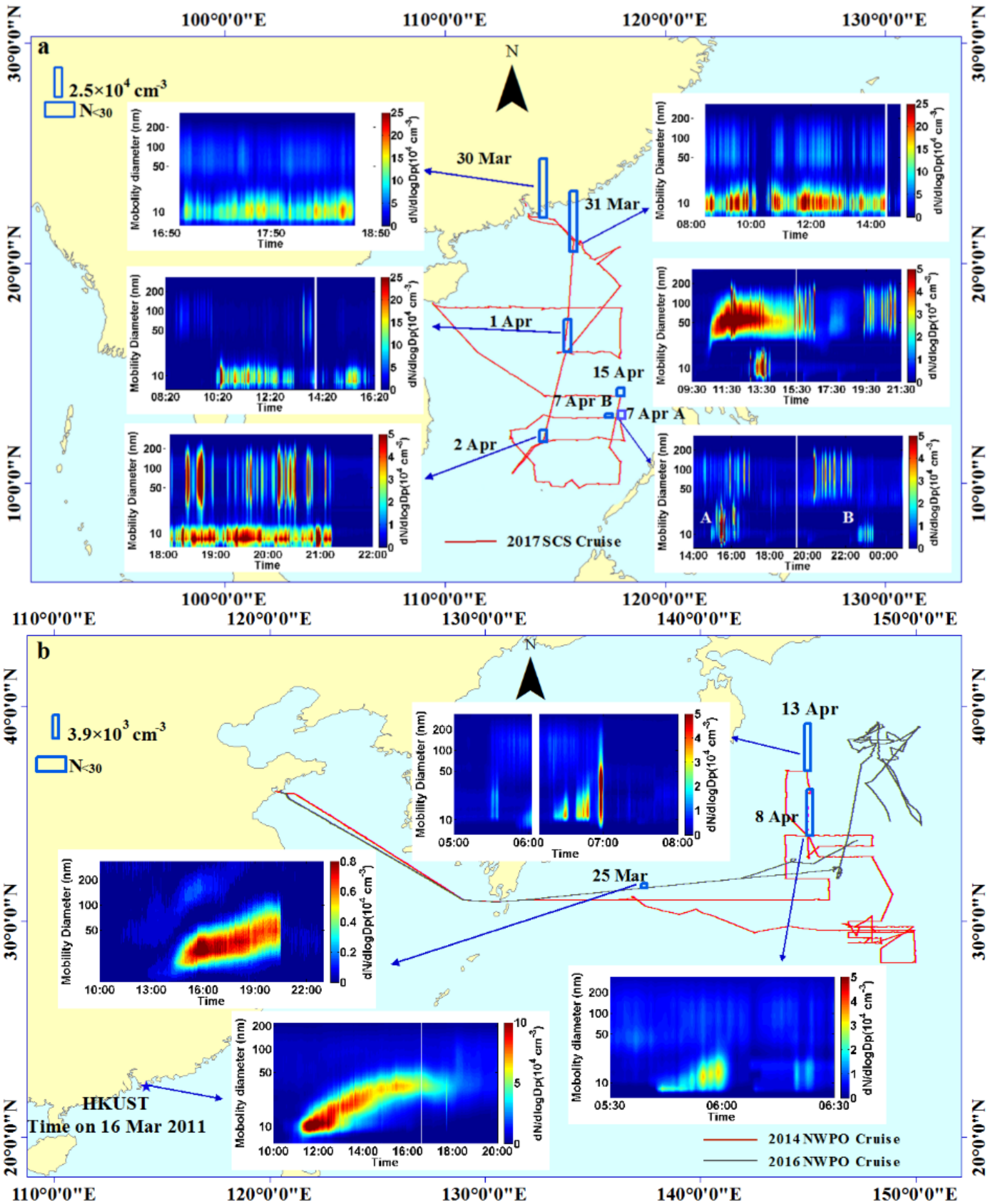

Fig. 1. NPF events observed in the atmosphere across SCS, NWPO and in Hong Kong. ((a) NPF events observed in the atmosphere across SCS, the blue bars represent the number concentration of the 5.6-30 nm particles ($N_{<30}$), the red line represents the cruise track across SCS during the period of 29 March to 2 May 2017; (b) NPF events observed in the atmosphere across NWPO in comparison with NPF in Hong Kong, the blue bars are defined as same as those across SCS, the red and gray lines represent the cruise track across NWPO in 2014 and 2016 individually.

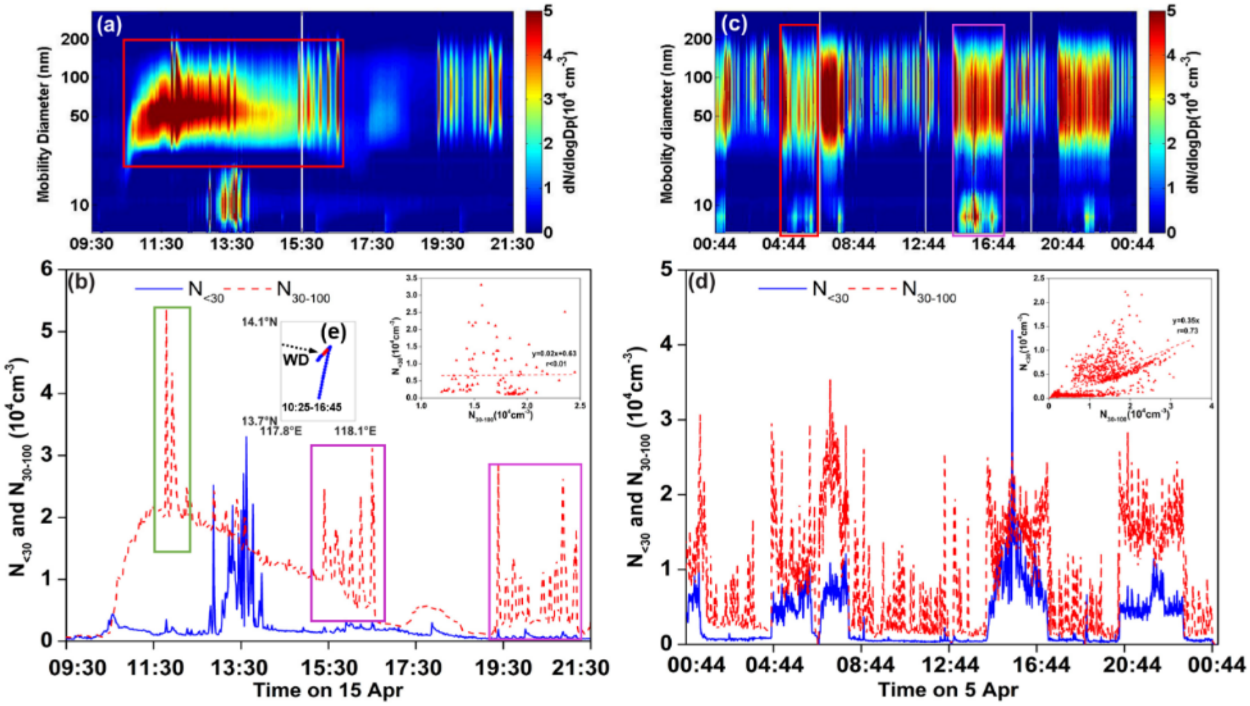

Fig. 2. NPF event observed on 15 April 2017 (left column) and plume observed on 5 April 2017 (right column) in the atmosphere across SCS. ((a), (c) contour plot of particles number concentration (d*N*/d log D_p); (b), (d) time series of $N_{<30}$ and $N_{30\text{-}100}$; (e) the vessel track at 10:25-16:45 superimposed in (b) and NPF was observed at the track of red line; the direction of the dotted arrow represents the predominant wind direction during NPF events.

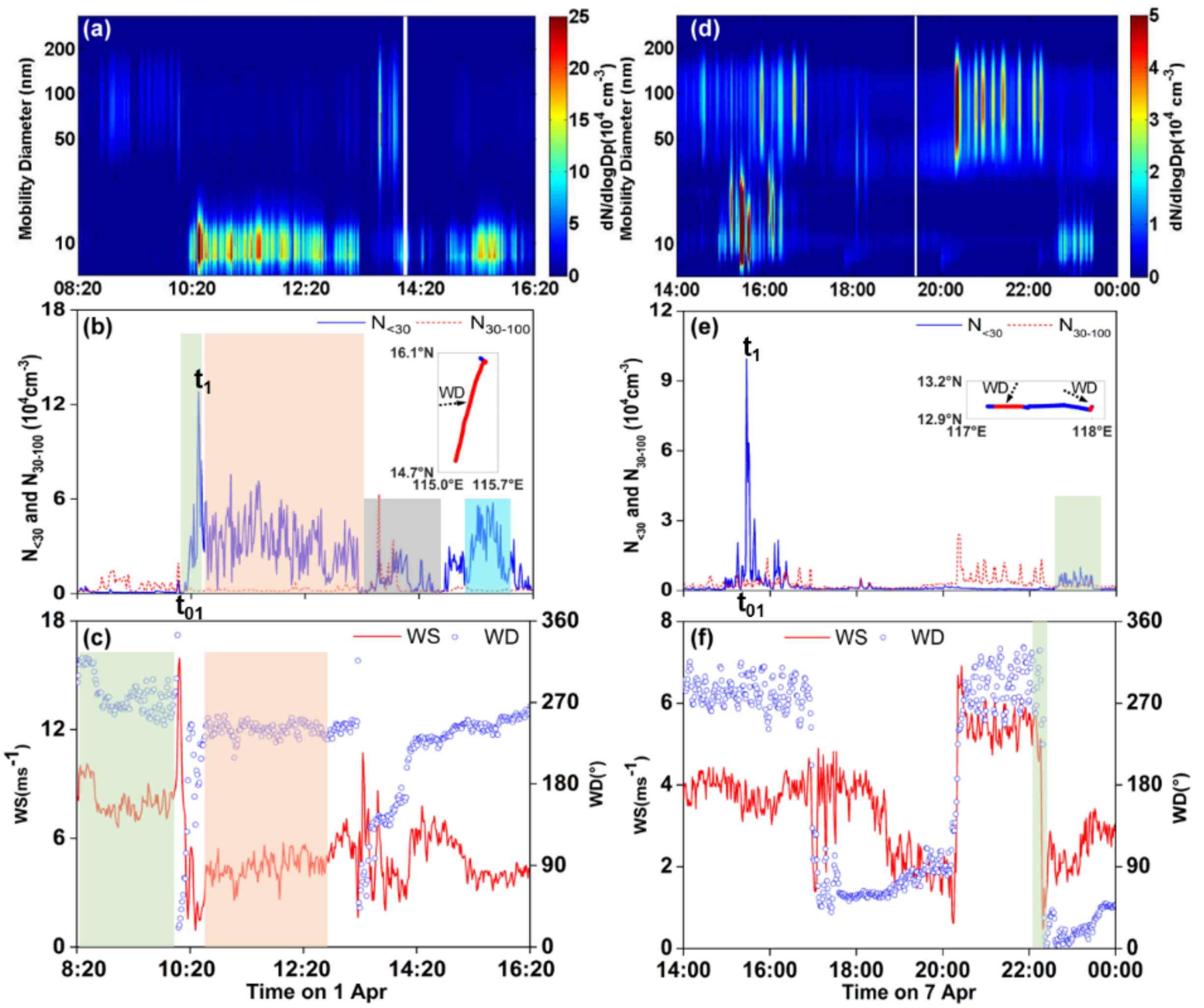

Fig. 3. NPF event observed on 1 (left column) and 7 April 2017 (right column) ((a), (d) contour plots particles number concentration (dN/d log D_p); (b), (e) time series of $N_{<30}$ and $N_{30\text{-}100}$; (c), (f) time series of wind direction and speed; The vessel track superimposed in (b) and (d), and red line is the track where NPF was observed; the direction of the dotted arrow represents the predominant wind direction during NPF events.

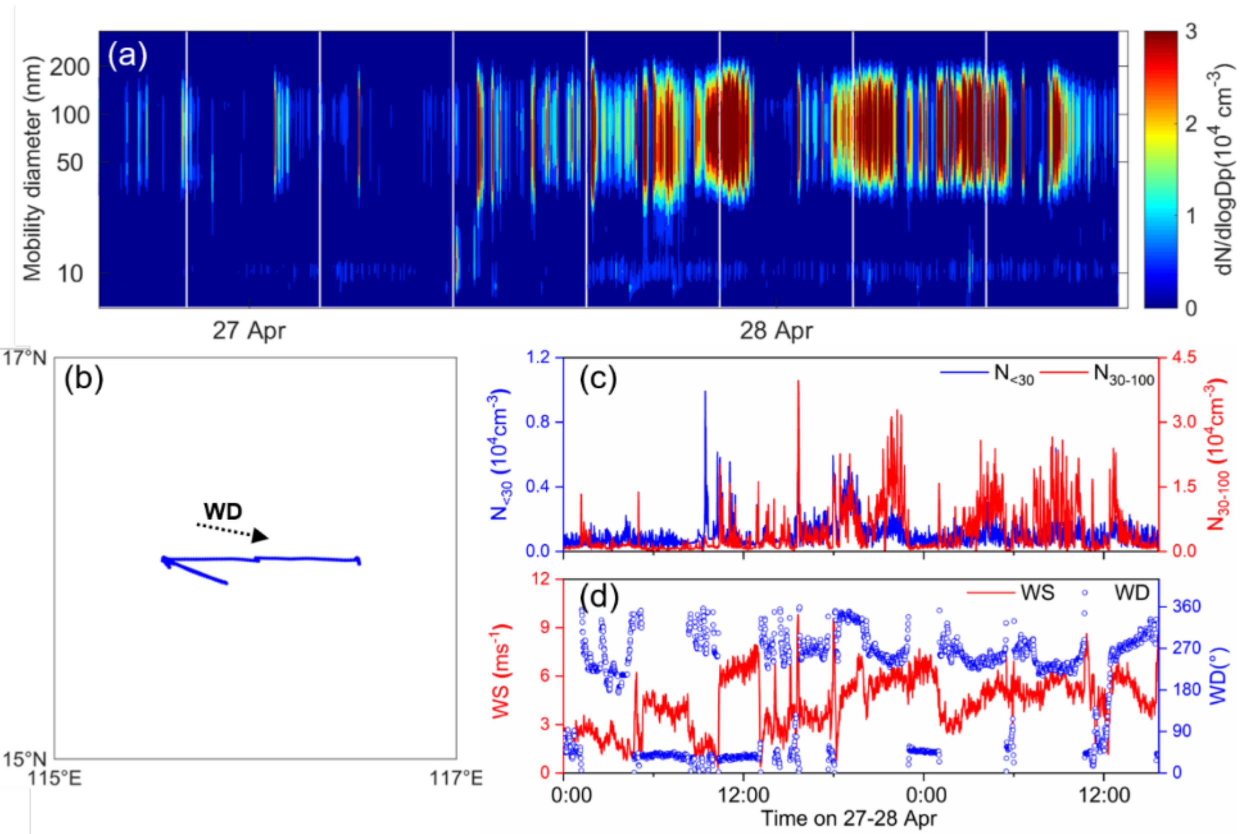

Fig. 4. Weak NPF events observed on 27-28 Apr. ((a) contour plots particles number concentration (dN/d log D_p); (b) The vessel track during 27-28 Apr and the direction of the dotted arrow represents the predominant wind direction during NPF events; (c) time series of $N_{<30}$ and N_{30-100}; (d) time series of wind direction and speed.

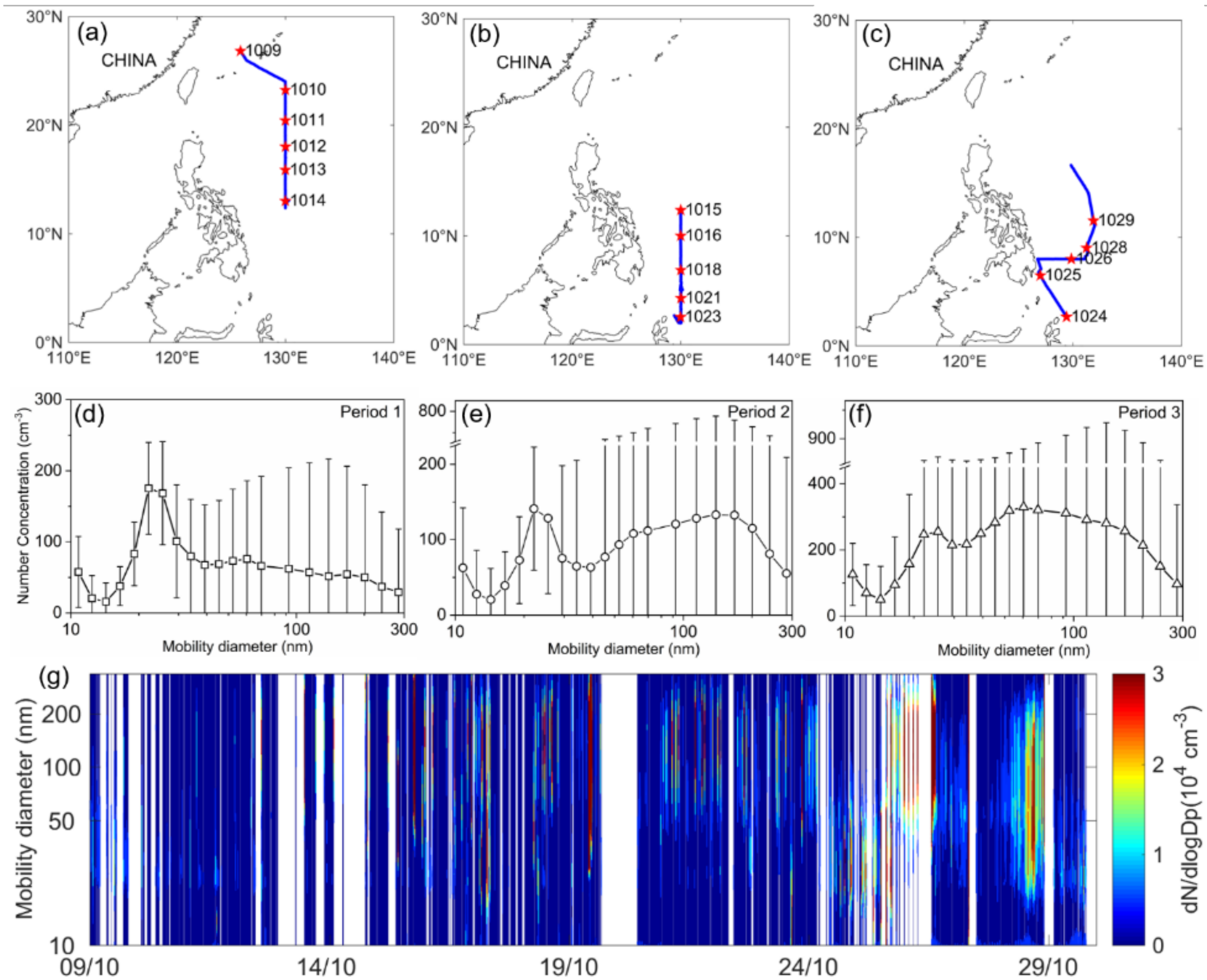

Fig. 5. (a), (b), (c) the vessel tracks during period 1 (09-14 Oct), period 2 (15-23 Oct) and period 3 (24-29 Oct) across NWPO in 2018; (d), (e), (f) particle size distribution during period 1, 2 and 3 respectively; (g) contour plots particles number concentration (dN/d log D_p) without self-vessel plume during 09-29 Oct across NWPO in 2018.

Table 1

Characteristics of NPF events observed across SCS and CVs for NPF events observed in the spring in Hong Kong

Place	event order	Date	Duration of NPF (h)	CS[&] ($10^{-2}ms^{-1}$)	NMINP (10^4 cm^{-3})	CVs (average ± standard deviation)								
						before NPF events			during NPF events			after NPF events		
						$N_{<30}$	N_{30-100}	ratios	$N_{<30}$	N_{30-100}	ratios	$N_{<30}$	N_{30-100}	ratios
SCS	1	30-Mar-17	>1.5	/	/	/	/	/	0.48± 0.19	0.21± 0.12	2.3	/	/	/
	2	31-Mar-17	>6.5	/	9.3*	1.16*± 0.48	0.32*± 0.08	3.6*	0.62± 0.32	0.27± 0.15	2.3	/	/	/
	3	1-Apr-17	6.5	2.2±1.36	6.5	0.48± 0.12	0.14± 0.03	3.4	0.74± 0.34	0.18± 0.10	4.2	/	/	/
	4	2-Apr-17	>3	/	/	/	/	/	0.74± 0.18	0.77± 0.25	0.95	1.32± 0.18	0.73± 0.13	1.8
	5	7-Apr-17	2	0.9±0.50	4.0	1.18± 0.17	0.37± 0.08	3.2	0.67± 0.24	0.50± 0.11	1.3	/	/	/
	6	7-Apr-17	1	1.1±0.38	0.7	/	/	/	0.69± 0.24	0.55± 0.13	1.3	0.96± 0.16	0.64± 0.13	1.5

	7	15-Apr-17	1.5	4.1±2.14	2.1	0.57±0.14	0.10±0.13	5.5	0.50±0.14	0.04±0.03	11	0.54±0.08	0.06±0.02	8.4
Hong Kong		16-Mar-11				0.07±0.03	0.03±0.01	2.3	0.01±0.01	0.02±0.01	0.5	0.05±0.01	0.02±0.01	2.5
		17-Mar-11				0.13±0.03	0.02±0.01	6.5	0.02±0.02	0.02±0.01	1	0.07±0.05	0.02±0.01	3.5
		25-Mar-11				0.30±0.08	0.02±0.01	15	0.07±0.03	0.02±0.01	3.5	0.12±0.02	0.02±0.01	6
		28-Mar-11				0.24±0.06	0.03±0.02	8	0.03±0.04	0.04±0.06	0.75	0.07±0.04	0.02±0.01	3.5
		6-Apr-11				3.6±1.6	0.03±0.01	120	0.10±0.06	0.03±0.01	3.3	0.09±0.03	0.03±0.02	3
		25-Apr-11				0.17±0.06	0.04±0.01	4.3	0.05±0.02	0.02±0.01	2.5	/	/	/

Note: "&" CS represents condensation sink and is calculated according to the method presented by Kumula et al. (2004); "/" means the value cannot be estimated, "*" means the calculation was estimated during part of one NPF event.

Graphical Abstract